



저작자표시-비영리-변경금지 2.0 대한민국

이용자는 아래의 조건을 따르는 경우에 한하여 자유롭게

- 이 저작물을 복제, 배포, 전송, 전시, 공연 및 방송할 수 있습니다.

다음과 같은 조건을 따라야 합니다:



저작자표시. 귀하는 원저작자를 표시하여야 합니다.



비영리. 귀하는 이 저작물을 영리 목적으로 이용할 수 없습니다.



변경금지. 귀하는 이 저작물을 개작, 변형 또는 가공할 수 없습니다.

- 귀하는, 이 저작물의 재이용이나 배포의 경우, 이 저작물에 적용된 이용허락조건을 명확하게 나타내어야 합니다.
- 저작권자로부터 별도의 허가를 받으면 이러한 조건들은 적용되지 않습니다.

저작권법에 따른 이용자의 권리는 위의 내용에 의하여 영향을 받지 않습니다.

이것은 [이용허락규약\(Legal Code\)](#)을 이해하기 쉽게 요약한 것입니다.

[Disclaimer](#)

Effects of SiC nanofluid on reflow heat transfer and hydrodynamic cavitation on its crud-like deposition for light water reactors

The background features a large, light gray watermark of the UNIST logo. It consists of a circular emblem with the text 'UNIST NATIONAL INSTITUTE OF SCIENCE AND TECHNOLOGY' around the perimeter. Inside the circle is a stylized 'U' shape containing a globe and a network diagram. Below the circle is a trapezoidal base with the word 'UNIST' written on it.

Seong Man Kim

Nuclear Science and Engineering Program
Graduate school of UNIST

2013

Effects of SiC nanofluid on reflood heat transfer and
hydrodynamic cavitation on its crud-like deposition
for light water reactors

Seong Man Kim

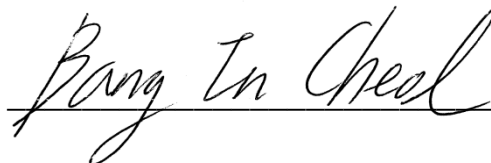
Nuclear Science and Engineering Program
Graduate school of UNIST

Effects of SiC nanofluid on reflood heat transfer and hydrodynamic cavitation on its crud-like deposition for light water reactors

A thesis
submitted to the Graduate School of UNIST
in partial fulfillment of the
requirements for the degree of
Master of Science

Seong Man Kim

02. 06. 2013
Approved by

A handwritten signature in black ink, reading "Bang In Cheol", written over a horizontal line.

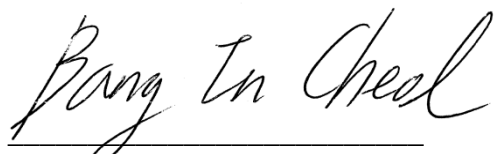
Major Advisor
In Cheol Bang

Effects of SiC nanofluid on reflood heat transfer and hydrodynamic cavitation on its crud-like deposition for light water reactors

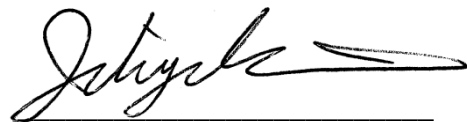
Seong Man Kim

This certifies that the thesis of Seong Man Kim is approved.

02. 06. 2013



Thesis Supervisor: In Cheol Bang



Ji Hyun Kim: Thesis Committee Member #1



Hyung Wook Park: Thesis Committee Member #2

Abstract

Efficiency and safety have been considered as the one of the important factors in the nuclear power plant. To enhance the efficiency and safety of the nuclear power plant, the heat transfer between fuel rods and coolant is important. For that reason, many researchers have been studying the heat transfer phenomena of the fuel rod in view of the coating layer. To analyze and resolve the coating effect in the fuel rods, this study consists of two parts of reflooding using nanofluids and removal test of crud using the cavitation.

Nanofluids were engineered by dispersing nanoparticles having high thermal conductivity into conventional heat transfer fluids. Because of these nanoparticles, the heat transfer performance of the fuel rod having coated surface is improved. This attractive property ensures that nanofluids can play an important role as a coolant of the heat removal by quenching the fuel rod during LOCA (Loss of Coolant Accident). Generally, the quenching experiments have been performed using the heated sphere and rodlet in the water and nanofluid (2-6). The results show the enhanced cooling performance like shifted cooling curve and reduced cooling time. Several quenched specimens that were exposed to high temperature in the working fluid have been gradually reducing the quenching time. Enhanced cooling performance was due to the specimen's structure with both dispersed and coated nanoparticle. This result shows the feasibility of nanofluid to adapt in ECCS (Emergency Core Cooling System) and primary system. During LOCA, the heated fuel rod is rapidly contact with coolant and particles of nanofluid will be attached on the fuel rod surface. The surface coated these nanoparticle shows porosity. It is similar with crud. In nuclear power plant, crud is known as composition of corrosion and oxidation materials. It has a porous structure which is combined with boron that is injected into the coolant for control of the power levels. The buildup of corrosion products on the fuel cladding surface has proven to be particularly significant for both BWRs and PWRs. The high temperature of the cladding surface attracts impurities and chemical additives in the reactor coolant that were deposited on the fuel rod surface in the process. The deposits on a fuel rod, known as crud, can be tenacious, insulative that one compounds capable of increasing the local clad temperature and accelerating clad corrosion—sometimes to the point of fuel failure. Crud composition on fuel cladding surfaces causes uneven heating of the reactor core. The situation is exacerbated by boron and added to the coolant to control power levels.

In Part I, to observe the quenching phenomenon of nanofluids, the test facility with a long vertical tube was designed and made. The experiments were conducted by using 0.01% volume fraction SiC/water and GO (Graphene Oxide)/water nanofluids as a coolant. By performing the experiments, the heat transfer performance of nanofluids were observed and compared to water. Compared with

deionized water, the cooling time of nanofluids was reduced 20 sec from and approximately 20 degree of contact angle on the tube was smaller.

In Part II, the possibility of removing the crud was studied using deposition like crud which is coated by SiC nanofluid and is exposed in the cavitation at each cavitation number. To optimize the removal effect, two type of flow was conducted as like common orifice flow and swirl orifice flow. In the case of experiment, the maximum shock pressure was gained during swirl flow at low cavitation number. It shows the concentrated pressure on pressure film than common flow. And, it shows maximized erosion effect at cavitation number 0.6.

Adoption of nanofluid to research the probability of SiC/water nanofluid and GO/water nanofluid can attribute to enhance the fuel performance in point of efficiency caused by enhanced cooling performance. Undesired specimens, as like crud, can be removed by cavitation phenomenon. In order to adopt cavitation, length of cavitation cloud should be considered to optimize the removal effect, because collapsing cavitation bubble is following the cavitation cloud length and the cavitation number. And SiC cladding material can bear the cavitation flow at above the cavitation number 0.7.

Contents

I.	Introduction -----	1
	1.1 Background -----	1
	1.2 Objectives -----	3
II.	Literature Study -----	4
	2.1 General Characteristics of Nanofluid -----	4
	2.2 Reflooding -----	7
	2.3 Mechanism of Entrainment -----	9
	2.4 Characteristic of crud -----	10
	2.5 Characteristic of Cavitation -----	12
	PART A. Nanofluid on Reflood Heat Transfer -----	22
III.	Experiments of Reflooding on Long Vertical Tube -----	23
	3.1 Preparation of Nanofluid -----	23
	3.2 Reflood Test -----	25
IV.	Results and Discussion -----	31
	4.1 Comparisons of Quenching Performance -----	31
	4.2 Analysis of Specimens -----	33
	PART B. Hydrodynamic Cavitation on its Crud-like Deposition -----	47
V.	Experiments of Hydrodynamic Cavitation -----	48
	5.1 Cavitation Simulation Facility -----	48
	5.2 Preparation of Coated Specimens -----	50
	5.3 Measurements of Shock Pressure -----	51

VI.	Results and Discussion -----	52
	6.1 CFD analysis -----	52
	6.2 Image of Bubble Flow -----	53
	6.3 Pressure Film -----	54
	6.4 Sample Test-----	55
VII.	Summary & Conclusions -----	70
	Acknowledgement-----	73

List of figures

Figure 1. The reflood phase in a PWR. In the dispersed flow regime the droplets impinge on the fuel rods without wetting (24).

Figure 2. Schematic diagram of heat transport during wick boiling. q_e is the evaporative heat flux and q_c the conductive heat flux (26).

Figure 3. Temperature across the deposit for a 35 and 59 μm thick deposit. Calculation with 2 ppm Li, 1200 ppm B and $25 \text{ cm}^3\text{kg}^{-1}$ (STP) H_2 (26).

Figure 4. Temperature at the bottom of the crud for different crud thicknesses, at different bulk water boron concentrations (26).

Figure 5. Cumulative mass loss vs time ($V = 49.0 \text{ m/s}$) (28).

Figure 6. Cumulative mass loss vs. time ($V = 36.3$ and 26.0 m/s ; uncertainty in cumulative mass loss, $\pm 0.05 \text{ mg}$) (28).

Figure 7. Effect of cavitation number σ on the M DPR (uncertainty in M DPR, $\pm 0.2 \mu\text{m/h}$): \circ , $V = 49.0 \text{ ms}^{-1}$; \bullet , $V=36.3 \text{ m/s}$; \bullet , $V=26.0 \text{ m/s}$ (28).

Figure 8. Cavitation cloud length vs σ (uncertainty in cloud length, $\pm 1 \text{ cm}$): \circ , $V = 49.0 \text{ ms}^{-1}$; \bullet , $V=36.3 \text{ m/s}$; \bullet , $V=26.0 \text{ m/s}$ (28).

Figure 9. SEM images of nanoparticles : (a) GO and (b) SiC.

Figure 10. TEM images of nanoparticles : (a) GO and (b) SiC.

Figure 11. Zeta potential as a function of pH in case of GO/water nanofluid.

Figure 12. Zeta potential as a function of pH in case of SiC/water nanofluid.

Figure 13. The reflood test apparatus.

Figure 14. Wall temperature variations during water reflood.

Figure 15. Wall temperature variations during SiC/water nanofluid reflow.

Figure 16. Wall temperature variations during GO/water nanofluid reflow.

Figure 17. Wall temperature variations during water and SiC/water nanofluid.

Figure 18. Wall temperature variations during water and GO/water nanofluid.

Figure 19. Wall temperature variations during water, SiC/water nanofluid and GO/water nanofluid

Figure 20. Macroscopic observations of the inner surface of the test section after the quenching experiments: (a) water, (b) SiC/water nanofluid and (c) GO/water nanofluid.

Figure 21. SEM observations of the inner surface of the test section after the quenching experiments: (a) water, (b) SiC/water nanofluid and (c) GO/water nanofluid.

Figure 22. SEM-EDS results of the inner surface of the test section after the quenching experiments of SiC/water nanofluid.

Figure 23. SEM-EDS results of the inner surface of the test section after the quenching experiments of GO/water nanofluid.

Figure 24. Contact angles of the inner surface of the test section after reflooding experiments: (a) water (68.2°), (b) SiC/water nanofluid (51.1°), (c) GO/water nanofluid (43.1°).

Figure 25. Schematic of experiments (27),(32).

Figure 26. Bare sample: (a) optical image, (b) microscope image of 1,000x magnification.

Figure 27. SiC-coated sample: (a) optical image, (b) microscope image of 1,000x magnification.

Figure 28. Film holder.

Figure 29. Analysis of flow by CFD.

Figure 30. Bubble distribution and size at each flow state: (a) $V : 9.54 \text{ m/s}$, $DP: 1.830 \text{ bar}$; (b) $V : 10.27 \text{ m/s}$, $DP : 1.570 \text{ bar}$; (c) $V : 11.01 \text{ m/s}$, $DP: 1.798 \text{ bar}$; (d) $V : 11.74 \text{ m/s}$, $DP: 1.993 \text{ bar}$; (e) $V : 12.48 \text{ m/s}$, $DP: 2.287 \text{ bar}$; (f) $V : 13.21 \text{ m/s}$, $DP : 2.541 \text{ bar}$; (g) $V : 13.95 \text{ m/s}$, $DP: 2.876 \text{ bar}$;

Figure 31. Bubble size distribution.

Figure 32. Effect of cavitation number in cases of using the orifice: (a) $\sigma = 0.5$, (b) $\sigma = 0.6$, (c) $\sigma = 0.7$.

Figure 33. Effect of cavitation number in cases of using a combination of orifice and mixer: (a) $\sigma = 0.5$, (b) $\sigma = 0.6$, (c) $\sigma = 0.7$.

Figure 34. Compared each test section: (a) Takahashi et al. (27), (b) Nagaya et al. (32), (c) Our experiment (27),(32).

List of tables

Table 1. The comparison of quenching velocity during water, SiC/water nanofluid and GO/water nanofluid.

Table 2. Contact angles of the inner surface of the test section after reflooding experiments.

Table 3. Effect of cavitation on the orifice.

Table 4. Effect of cavitation in combination with the orifice and static mixer.

Table 5. Erosion effect of cavitation in combination with the orifice and static mixer.

Table 6. Shock pressure at the cavitation number on each experiment.

Nomenclature

C	heat capacity	[J/k]
D	diameter	[mm]
d	orifice diameter	[mm]
<i>d</i>	wall thickness	[mm]
<i>e</i>	thermal effusivity	$[(\rho Ck)^{1/2}]$
G	mass flux	[kg/ m ² ·s]
h	heat transfer coefficient	[W/m ² ·K]
k	thermal conductivity	[W/m·K]
P	pressure	[Pa or MPa]
t	wall thickness	[mm]
V	velocity	[m/s]
Z	distance from inlet plane	[m]

Greek symbols

ρ	density	[kg/m ³]
σ	cavitation number	
φ	concentration	
ε	thickness of heater (=radius/2)	[m]

Subscript

f	fluid
i	inlet
Le	Leidenfrost
o	orifice
p	particle
<i>QF</i>	quench front
s	static
S	saturation
v	vapor
W	Wall
wet	wetting
t	thickness

I. Introduction

1.1 Background

Improved cooling performance of the coolant is issued with a requirement to have high efficiency and safety in the nuclear power plant. The proper selection of the structure and the coolant is useful to enhance the cooling efficiency. However, the change of structure is physically limited. Furthermore, it is expensive to change the present component.

Therefore, research has been studied to enhance the cooling performance by altering the coolant characteristics. Nanofluid is one of the solutions to enhancing the heat transfer. In coolant system, nanofluids which contain the nanoparticle can enhance the heat transfer. However, it has disadvantages of working pressure. Their some results are that the heat transfer are increased with increase of nano-particle concentration

Numerous theoretical and experimental studies of suspensions containing solid particles have been conducted since Maxwell's theoretical work was published more than 100 years ago (8). However, due to the large size and high density of the particles, there is no good way to prevent the solid particles from settling out of suspension. The lack of stability of such suspensions induces additional flow resistance and possible erosion. Hence, fluids with dispersed coarse-grained particles have not yet been commercialized.

Recently development of working fluids extensively researched in engineering technology related to nuclear energy, vehicle engineering, electronic chips have interest in enhancement of heat transfer. As part of research, coolants are developed as more compatible method. Nanotechnology is one of the candidates of this process (1).

In primary system, coolant is interacting with fuel rods within this coolant worked as stabilizer of system. Fuel rod generates the high heat flux that is make high temperature. If it is not properly stabilized as marked temperature, it will be melted and make the damage of reactor. Therefore high heat flux must be stabilized and cooled as planed temperature. Water is one of the coolants as extensively used in the engineering technology. However, it has limitation caused by characteristic so that enhanced coolant is required. Utilized Zircaloy tube can make the hydrogen when fuel rods are exposed on high temperature. For preventing the accident, especially LOCA (Loss of Coolant Accident) is need to quickly stabilized for avoid the explosion. To avoid interaction with hydrogen, the best solution is method of stabilizing cooling system. Another method is the elimination of hydrogen before the explosion.

For power uprating, concentration of crud from a power management strategy view has been an issue within commercial nuclear power plants. Axial Offset Anomaly (AOA) referring to an unexpected

neutron flux depression is also known as a crud Induced Power Shift (CIPS). Fuel assemblies removed from an AOA core have shown a thick porous deposition layer of crud on the fuel clad surface. The deposition layer was induced by precipitation reactions of both boron species and crud during sub-cooled nucleate boiling. Therefore, to resolve the AOA issues, a fuel cleaning technology using ultrasonic cavitation has been developed by EPRI. Another solution to resolve the crud is chemical additive. The injection of soluble zinc additive to the reactor coolant has been used for the purpose of radiation field reduction, general corrosion control. Characteristic of zinc can inhibit crud growth. However, the performance of these methods is not enough.

1.2 Objectives

If coolant does not cool the nuclear reactor, fuel rod will be heated up. After these step, Zircaloy cladding will be interact with steam at 1400 K. An exothermic reaction occurs between steam and zirconium, which may produce enough heat to be self-sustaining even without the contribution of decay heat. Moreover, interaction between the Zircaloy and water can make the hydrogen. Therefore, hydrogen will must be emitted to the reactor core before that it makes the explosion. Hydrogen embrittlement may occur in the reactor materials and volatile fission products are released from damaged fuel rods.

For preventing this accident, enhanced coolant is required to the nuclear society. We think that nanofluid can be useful coolant for ECCS. There is a need to understand the characteristics of the investigation before determining the applicability of nanofluids. Measured quenching time will attribute the criteria of judgment as coolant during LOCA. Reduced quenching time is useful for the operator because the operator can gain the spare time for handling the accident. For that kind of possibility, our objective is measuring the quenching time and velocity to heated long vertical tube. The enhancing cause of the cooling performance after the quenching experiments using nanofluid were investigated through the macroscopic observation, scanning electron microscopy (SEM), contact angles and SEM-energy dispersive X-ray spectroscopy (EDS) of the inner surface of the test section. Most importantly, our experiments are able to similar the real fuel rod length. Other quenching experiment was conducted using the rodlet or sphere. These differences of length or structure cannot measure the possibility of entrainment. The aim of our experiment is to find the possibility of coolant when emergency cooling is required to cool the heated core. Also, the aim of our experiment is to verify the precursory coating by entrainment when quenchant is injected to the heated long vertical tube. Specimens coated nanoparticles are known as porous structure with loosely deposited layer. That kind of porous structure is appeared on the crud coated fuel rod. So, we used specimens coated SiC. The materials of SiC are a candidate of fuel rod. Crud consists primarily of magnetite, nickel ferrite, and cobalt ferrite. For the purpose of checking the cavitation effect in this work, however, specimens made of SS 316L are simply deposited by silicon carbide nanoparticles since the nanoparticles bond with the crud porous layer. It shows a crud-like deposition structure. To remove the crud-like deposition, we use the cavitation mechanism. The purpose of cavitation experiment is to find the possibility of cavitation when it is adjusted to the crud removal system. For that purpose of our research, cavitation effect was investigated through the shock pressure, cavitation number and erosion of specimens.

Therefore, our experiment will be contributing the distinction to the possibility of damage when removal test is adopted by cavitation.

II. Literature Study

2.1 General Characteristics of Nanofluid

Water is oldest working fluids in engineering. It can be easily gained and take advantage of handling. So, water is widely used in commercial usage. During the past, enhanced cooling performance has been required to adapt to the newly designed system for enhancing the efficiency and safety. In this requirement is the reason of developing of nanofluids. Nanofluids as new kinds of heat transfer fluids are a new class of nanotechnology-based heat transfer fluids engineered by dispersing nanoparticles into conventional heat transfer fluids. Nuclear society also uses the nanofluid for enhancing the power efficiency. Almost of research in nuclear engineering is concentrate to CHF (Critical Heat Flux). Flow boiling is partially focused field. That kind of research is conducted using the SiC (Silicon carbide), Al₂O₃ (Alumina oxide) and CNC (Carbon nano colloid). "Nanofluids" could be regarded as an alternative for the effective coolant in the various fields of industry. Those are a new class of nanotechnology-based heat transfer fluids engineered by dispersing nanoparticles into conventional heat transfer fluids such as water, ethylene glycol, and engine oil (1). Several researchers have carried out experiments to confirm the capabilities of nanofluids for a boiling heat transfer (2-6). The general consensus in their researches is that nanofluids enhance the critical heat flux (CHF) significantly, however, they have no significant effect on a heat transfer in a nucleate boiling region. Recent studies have shown that a CHF enhancement is attributed to a high wettability of a thin layer formed on a heating surface by a deposition of nanoparticles (9). The film boiling heat transfer rate in nanofluids was lower than that in the water for a sphere specimen (10). Nanoparticles deposition on the sphere surface resulted in quick quenching of the hot sphere (11, 12). More recently, the rodlet specimen with nanoparticles deposition led to the premature disruption of film boiling and quenching acceleration (12). Most of the studies on a heat transfer of nanofluids have been concentrated on the nucleate boiling region and the CHF phenomenon.

Kim et al. (11) studied experimentally the quenching for small metallic spheres exposed to pure water and Al₂O₃, SiO₂, diamond/water nanofluids at low concentrations (≤ 0.1 vol. %). The test specimens were made of stainless steel (SS) and zircaloy, and the initial temperature of test specimens was about 1,000 °C. The authors found that the film boiling heat transfer in nanofluids is almost identical to that in pure water. That is, the nanoparticles present in the nanofluids have no major effect on the quenching process. However, some nanoparticles deposit on the sphere surface during the quenching process can greatly accelerate the end of film boiling in subsequent quenching tests. So, they stated that the surface roughness increase and wettability enhancement may be responsible for the premature disruption of the film boiling and the acceleration of quenching due to nanoparticle deposition. Lotfi

and Shafii (10) performed transient quenching experiments on a high temperature silver sphere in Ag, TiO₂/water nanofluids to investigate boiling heat transfer characteristics of nanofluids. The initial temperature of test specimen was about 700 °C and the initial temperature of nanofluid was 90 °C. The authors found that the quenching process was more rapid in pure water than in nanofluids and the cooling time was inversely proportional to the nanoparticle concentration. They stated that nanoparticle deposition on the sphere surface acted as a thermal insulator for the sphere and reduced the temperature of the sphere outer surface, due to the higher thermal resistance of the TiO₂ layer. Also, nanoparticle deposition prevented a stable vapor film from forming around the sphere, which promoted the rapid quenching of the hot sphere. Kim et al. (12) studied the quenching characteristics of metallic rodlets and spheres in pure water and Al₂O₃/water nanofluids of 0.1% by volume. The experiments were performed in both saturated and subcooled conditions under atmospheric pressure. The authors found that the initial quenching behavior in nanofluids is identical to that in pure water, and the quench front speed is significantly enhanced in subsequent quenching repetitions due to nanoparticle deposition. They stated that the hydrophilic nature of the nanoparticle increases the area of the liquid–solid contacts during film boiling, which efficiently destabilizes the vapor film at higher temperatures and the very fast propagation of the quench front is also associated with local liquid–solid contacts during film boiling. Chun et al. (13) investigated the effects of Si and SiC nanofluids on a boiling heat transfer during a rapid quenching of a thin platinum (Pt) wire. The authors found that when the Si and SiC nanoparticle-coated Pt wires are quenched with the water, the nanoparticle-coated Pt wires are cooled down at a very high rate, compared to the bare Pt wires cooled by the water and the Si nanofluids. They stated that a considerably large heat transfer coefficient is obtained in a wide range of the wall superheat, compared to those of the bare Pt wires cooled by the water and the nanofluids during a quenching of the Si and SiC nanoparticle-coated Pt wires. Bolukbasi and Ciloglu (14) studied the pool boiling heat transfer characteristics of a vertical cylinder quenched by SiO₂/water nanofluids around a high temperature brass rod (diameter 20 mm × 75 mm) at saturated temperature and atmospheric pressure. The authors found that the pool film boiling heat transfer in nanofluids is identical to that in pure water, but, during the repetition tests in nanofluids with high concentrations, the film boiling region disappears, and the critical heat flux increases. They stated that the nucleate pool boiling heat transfer coefficient decreases compared with that of pure water, but a considerable decrease in nucleate pool boiling heat transfer is not observed with the repetition tests. The main reason for this decrease was the deposition of nanoparticles during the quenching tests. Ciloglu and Bolukbasi (15) studied the quenching behavior of aqueous nanofluids containing various volume fractions of Al₂O₃, SiO₂, TiO₂ and CuO nanoparticles around a high temperature brass rod (diameter 20 mm × 75 mm) at saturated temperature and atmospheric pressure. The authors showed that although it is not observed from the first run in nanofluids, the quenching time is considerably shortened during the repetitive quenching tests and the quenching process is strongly dependent on

the kind of nanoparticle, as well as its volume fraction. They stated that the characterization of the nanoparticles deposition layer showed an increase in the surface roughness and a decrease in contact angle, which was the primary reason for CHF enhancement. In addition, the results showed that there was no considerable change in nucleate boiling heat transfer for all nanofluids. Lee et al. (16) conducted the reflood heat transfer experiments to investigate the effect of 0.1 volume fraction (%) Al_2O_3 /water nanofluid and carbon nano colloid (CNC) in the tube (1,000 mm in the heating length). The authors showed that the cooling performance is enhanced by more than 13 seconds and 20 seconds for Al_2O_3 /water nanofluid and CNC, respectively. They concluded that a more enhanced cooling performance is attributed to a high wettability of a thin layer formed on a heating surface by a deposition of nanoparticles and the thin layer deposited nanoparticles is formed because the vapor including nanoparticles is deposited on heating surface before fluids are moved, when fluids are moved from bottom to top during reflood. Also, they concluded that a more enhanced cooling performance can be achieved by decreasing the amount of hydrogen at the severe accident.

2.2 Reflooding

In the LOCA, the surface temperature on fuel rod is toward to the undesired temperature that is can be melting temperature of fuel material. Therefore, contained radioactive materials have possibility of leaking. So it must be rapidly cooled for preventing the severe accident. During the design of nuclear power system, engineers consider the preventing system for treating the undesired accident. LOCA is not another story. ECCS is one of the safety systems in the NPP (Nuclear power plant) which is designed to automatically maintain the system. Phase change of coolant provides the unpredictability. Therefore phase change of water interaction with heated wall is important as part of the research the ECCS. Vapor has low thermal conductivity compared to water state. So, if surface has enhanced possibility of wettability, heated wall can be easily avoiding the peaking temperature locally. Moreover, temperature can be more easily stabled because vapor doesn't interrupt the flow.

Rewetting during the reflood is important to establish normal and safe condition of nuclear fuel rods. It is the re-contact of liquid with hot surface. A quench front (QF) means the edge of the contact area. On this area, advancing progressive cooling of surface is occurred than other point and temperature is approached to the saturation temperature (17). A quench velocity shows advancing velocity of the boundary and the apparent temperature. In this area, surface of nuclear fuel rod starts to be cooled quickly in a short time. Therefore, quench front and rewetting are important to analyze the quenching performance. Apparent temperature (apparent rewetting temperature or quench temperature) established by the intersection of tangent lines to the 'knee' of the measured temperature-time trajectories at the point where its slope is the largest, with the tangent to the curve before quenching are correlated by Kim and Lee (18). This temperature indicates the onset of a rapid surface cooling caused by an enhanced rate of heat transfer that does not necessitate liquid-solid contact. The rewetting temperature is formed in the gas-liquid-solid area. The apparent temperature is predicted as shown in Equation 1. It is function of the wall properties, wall initial temperature and the coolant inlet temperature and mass flux. Where k , ρ and C are the wall conductivity, density and specific heat respectively, d is the wall thickness and Z is elevation.

$$\frac{T_{AR} - T_S}{T_W - T_S} = 19.51 \left(\frac{T_S - T_{in}}{T_W - T_S} \right)^{0.107} \left[\left(\frac{Ct}{k} \right)_W G \right]^{-0.162} \times \left[\left(\frac{k\rho}{d} \right)_W \frac{T_W - T_S}{G^3} \right]^{-0.0989} \left(\frac{Z}{t} \right)^{-0.163} \quad (1)$$

Apparent temperature and rewetting phenomenon can explain the effects of nanofluids results. Quench velocity can be explained approximately by two equation. It is derived from a two-

dimensional Fourier equation of heat conduction by Duffey and Pothouse (19).

For $Bi \ll 1$,

$$u_{QF}^{-1} = \rho C \left(\frac{\varepsilon}{h_{QF} k} \right)^{1/2} \frac{(T_{wet} - T_s)^{1/2} (T_{wet} - T_{Le})^{1/2}}{(T_{Le} - T_s)} \quad (2)$$

For $Bi \gg 1$,

$$u_{QF}^{-1} = \frac{\pi \rho C k}{2 h_{QF}} \cdot \frac{(T_{wet} - T_s)}{(T_{Le} - T_s)} \quad (3)$$

If nanofluid has larger heat transfer coefficient than water in apparent temperature or Leidenfrost temperature, results can be expected that quench velocity would be increased.

2.3 Mechanism of Entrainment

Droplet of fluids is acted as heat sink and can entrain the some particle. When the LOCA is occurred, heated wall will be cooled by reflooded working fluid. Before interacting coolant with top of component, precursory cooling is achieved by superheated vapor with entrained droplet. That kind of droplet heat transfer with correlation was studied for analyze the cooling process to adopt the variety phenomenon. Lee et al. (20) studied size and number density change in regard to reflood. The evaporation rate of droplet populations is analyzed by taking into account the relevant convective and radiative heat transfer mechanism. This research can explain the energy transfer from the cladding surface in the vicinity above the quench front.

Early dispersed flow models assumed thermodynamic equilibrium conditions between liquid and phases (21, 22, 23). Chatzikyriakou et al. (24) studied correlation between droplet velocity and heat loss per droplet interaction. According to the study, interaction does not depend on the approach velocity. When LOCA is occurred, heated wall will be cooled by reflooded working fluid. Before cooling of the quench front through wetting by coolant, entrainment which is occurred by reflood due to the interaction between coolant and heated wall at the downward is generated. In this process, upward component interact with entrained vapor and particle as shown in Figure 1.

2.4 Characteristic of crud

The nuclear industry has concerned about operational safety and power efficiency. For this, cleaning is one of the processes of maintenance that is conducted to remove the crud that builds up to on the fuel surfaces within the reactor core activated by neutrons to form radioactive nuclides. That is made up of corrosion material on cladding surface and it can lead to Axial Offset Anomaly (AOA). AOA is known as neutron flux depression in the top of the nuclear reactor. This phenomenon makes it difficult to operate and decontaminate the reactor. In this case of crud, unpredicted occurrence is related with interaction of boron, because boron is deposited within the porous crud layer. Originally boron is injected to coolant for control the power. However, it interrupts the flux of fuel as results of neutron absorption by boron within crud layer on fuel surface. That kind of crud has the adhesive deposition that is deposited by subcooled nucleate boiling during the circulation of coolant. As result of deposition, fuel assembly which has crud layer will be occurs AOA. AOA cause the reactor trip and worker's exposure of radiation will be increased.

For solving the problem, researchers investigated the property of crud. However, property of crud has various compositions because it is affected by surrounding environment.

Pan et al. (25) investigate correlation between the concentration levels of solute and wick boiling condition. As results of research, concentration decreased with increasing distance from chimney wall at a given axial location and heating surface at a given radial location. Another result is maximum concentration increased with decreasing porosity under some condition as like increasing chimney population density and increasing system pressures.

Henshaw et al. (26) studied using the model which is described for simulating thermal hydraulic and chemical conditions within fuel crud deposits. In this study, authors consider the transport and chemist of dissolved species within the deposit. Furthermore, chemistry includes equilibrium chemistry of Li/boric acid species, the equilibrium chemistry of Fe/Ni species and the radiolysis chemistry of water. For simulating heat transfer and wick boiling model, Figure 2 is used in this research.

Figure 3 shows how the temperatures varies through the crud for a 35 and 59 μm thick deposit. It is indicating the rise in species concentrations towards the bottom of the crud causes a rise in the saturation temperature and because the solubility of LiBO_2 falls with increasing temperature it precipitates. And added results show how the temperature at the bottom of the crud deposits changes with crud thick ness and bulk water boron concentration as shown in Figure 4.

To decrease the effect of crud, method of removal was investigated. It is divided into two ways. One is the elimination of crud. Another is the inhibition of growth. Method of elimination is divided again as chemical method and ultrasonic method. Chemical method is applied to the metal using the corrosive fluids. This method also can remove the polluted material, however, used fluid also polluted during the process. Therefore radioactive material is increased as results of removal. Ultrasonic

method is widely used. It is developed by EPRI (Electric Power Research Institute) for removing deposits on fuel assemblies.

2.5 Characteristic of Cavitation

Cavitation is known as hydrodynamic mechanism and can erode the mechanical component when it is occurred. From a technical stand point, crux of the problem is that most of component in the flow system are not equipped to prevent cavitation occurrence. Severe erosion and rupture can be occurred when component be exposed on explosive cavitation. There are many options available for preventing erosion caused by cavitation. Cavitation occurred from the impeller and is easily identified. Pressure drop caused by increase of flow velocity in flow region can cause a cavitation. Pressure is inverse proportion to the velocity. Therefore, when screw rotate along the axial direction, increased velocity around the impeller can make the pressure drop, cavitation will be generated and be collapsed. When pressure is decreased as vapor pressure in the flow region, bubble can be generated. In reverse proceed, bubble will be disappeared. Finally, collapsed cavitation generates shock pressure. At this process, surface of component is eroded and broken gradually. For this reason engineers researched about cavitation to prevent the problem.

Cavitation is made in other ways as ultrasound method. It can be called as ultrasound cavitation or ultrasonic cavitation. It is based on the resonance of pressure waves in continuous transmission. At procedure, compression and depressurization are repeatedly occurred. In short, cavitation mechanism occurs when there is pressure gradient. If proceed consistently would take place in region, bubble of cavity is more compressed and take the high energy. Finally bubble will be collapsed when it is more warped by surrounding environment.

To characterize the cavitation effect, it was investigated by many standards like shock pressure or noise, oscillation of the vibrator, and erosion of the sample. In this experiment, we considered the shock pressure for its decontamination effect, which can be associated with erosion. Takahashi et al. (27) investigated the shock pressure distributions using a sensitive pressure film. Cavitation was generated by three types of orifices. It was installed at the middle of the test section. The results show the relation among the maximum shock pressure and the cavitation number as well as its position. Hattori et al. (28) studied the erosion effect caused by the collapse of cavitation in the venturi facility. Venturi cavitation erosion tests were performed and correlated with the bubble collapse pulse height spectra measured by a microtransducer. The effects of the throat velocity and the cavitation number σ (referred to the downstream pressure and throat velocity) on the erosion rate (MDPR: Mean depth of penetration rate) were studied. Fan et al. (29) analyzed the effect of nanobubbles on froth flotation. Nanobubbles were generated by a cavitation tube and static mixer. The tests were performed to evaluate eight important parameters governing the median size and the volume of nanobubbles. These process parameters included surfactant concentration, dissolved oxygen (O_2) content, and dissolved carbon dioxide gas (CO_2) content, pressure drop in cavitation tube nozzle, hydrophobic particle concentration slurry temperature and the time interval after nanobubble generation. Vickers and

Houlston (30) characterize some parameters in the cavitation cleaning jet. In this study, a model is presented of the erosion damage and cleaning efficiency of cavitation and conventional cleaning jets. The effect of supply pressure, jet velocity, standoff distance, nozzle diameter and type of fluid are considered and assessed in relation to experimental findings.

These cavitation show some relations between cavitation number and erosion rate. Mass loss of specimens is increased along the increasing cumulative time. Mass loss increased with increasing cumulative exposure time. Above the cavitation number 0.72, mass loss does not depend on time. Only cavitation number 0.6 depends on cumulative time as shown in Figure 5 and 6. That kind of dependency of cavitation number is also related with MDPR. MDPR is effectively shown between cavitation number 0.6 and 0.8. When cavitation is occurred, micro and nano-bubble can be observed. These bubbles are concentrated within some length. According to Figure 8, these cloud length was observed within 15 cm. It shows the cloud length is related with MDPR.

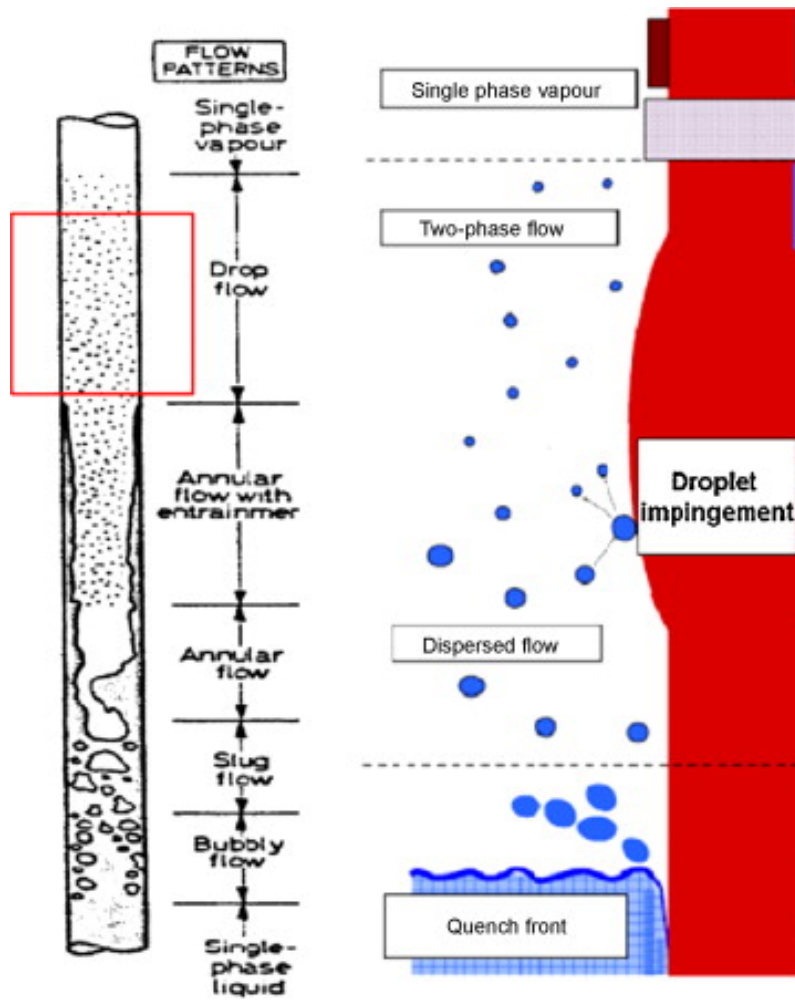


Figure 1. The reflood phase in a PWR. In the dispersed flow regime the droplets impinge on the fuel rods without wetting (24).

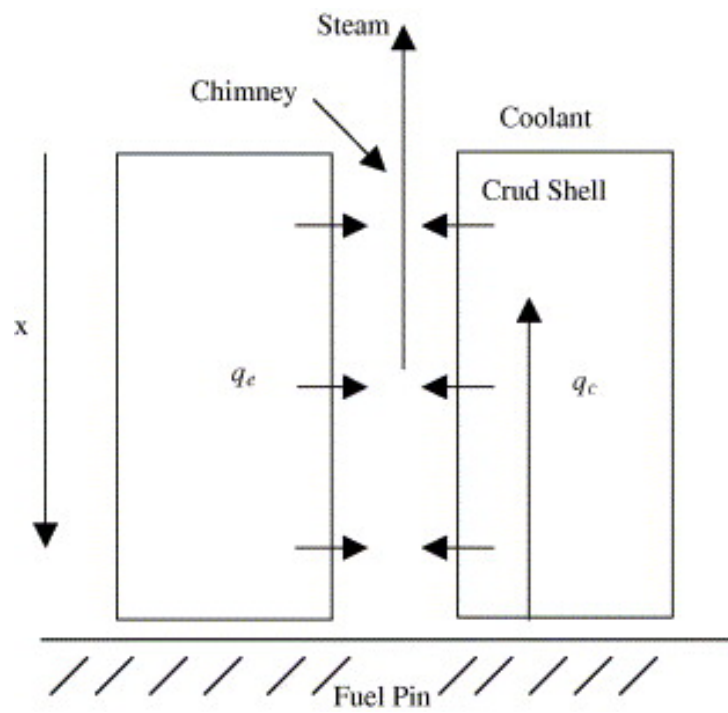


Figure 2. Schematic diagram of heat transport during wick boiling. q_e is the evaporative heat flux and q_c the conductive heat flux (26).

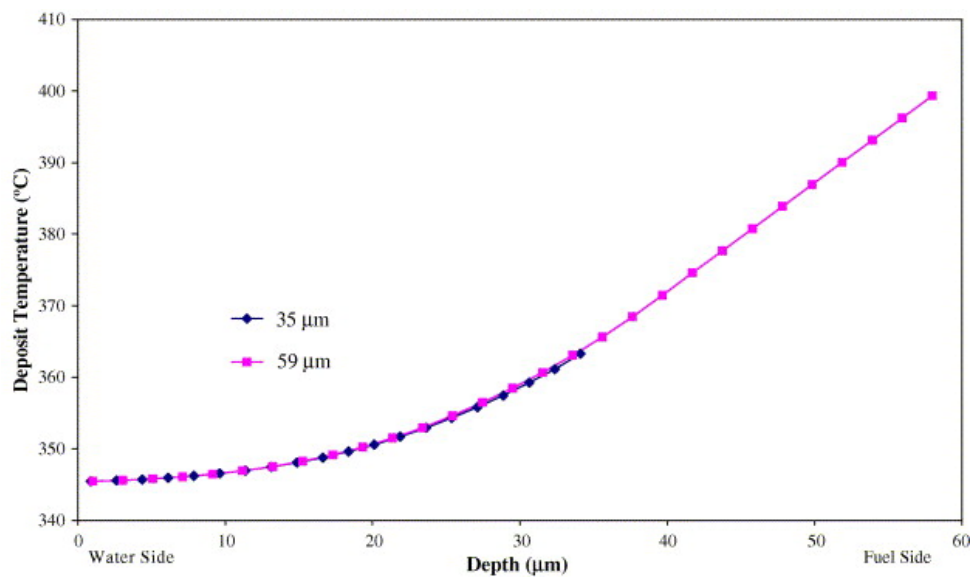


Figure 3. Temperature across the deposit for a 35 and 59 μm thick deposit. Calculation with 2 ppm Li, 1200 ppm B and 25 cm³ kg⁻¹ (STP) H₂ (26).

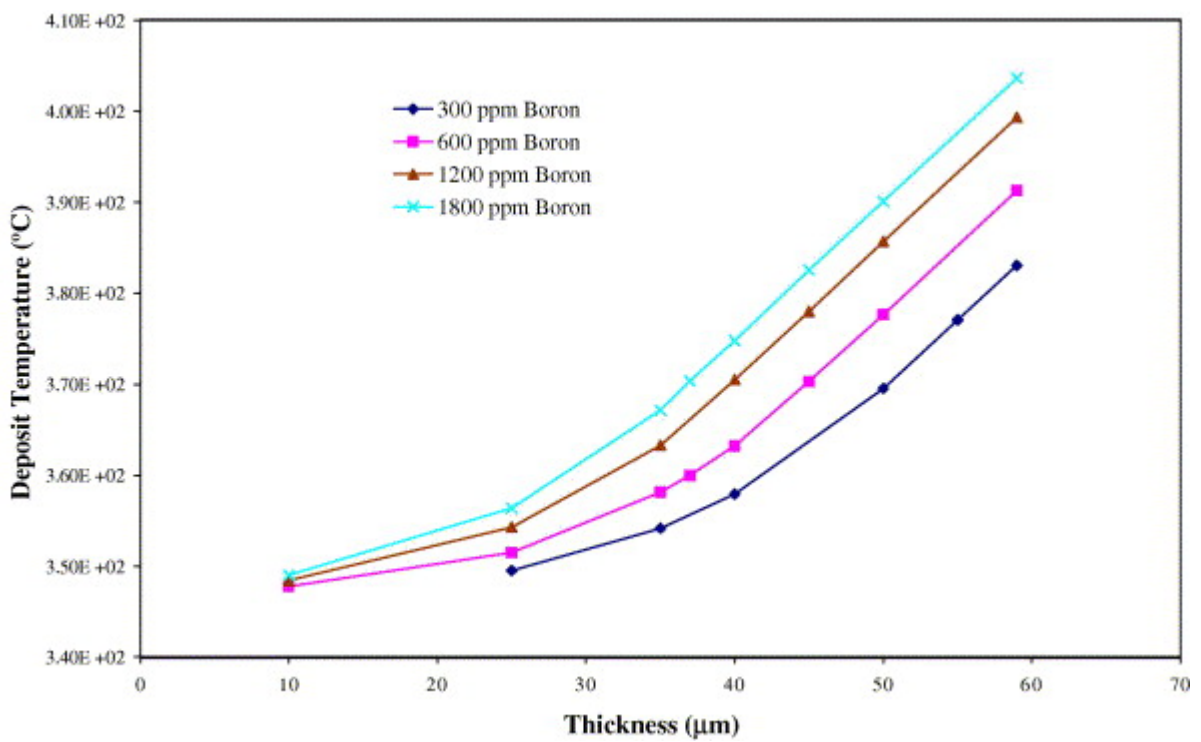
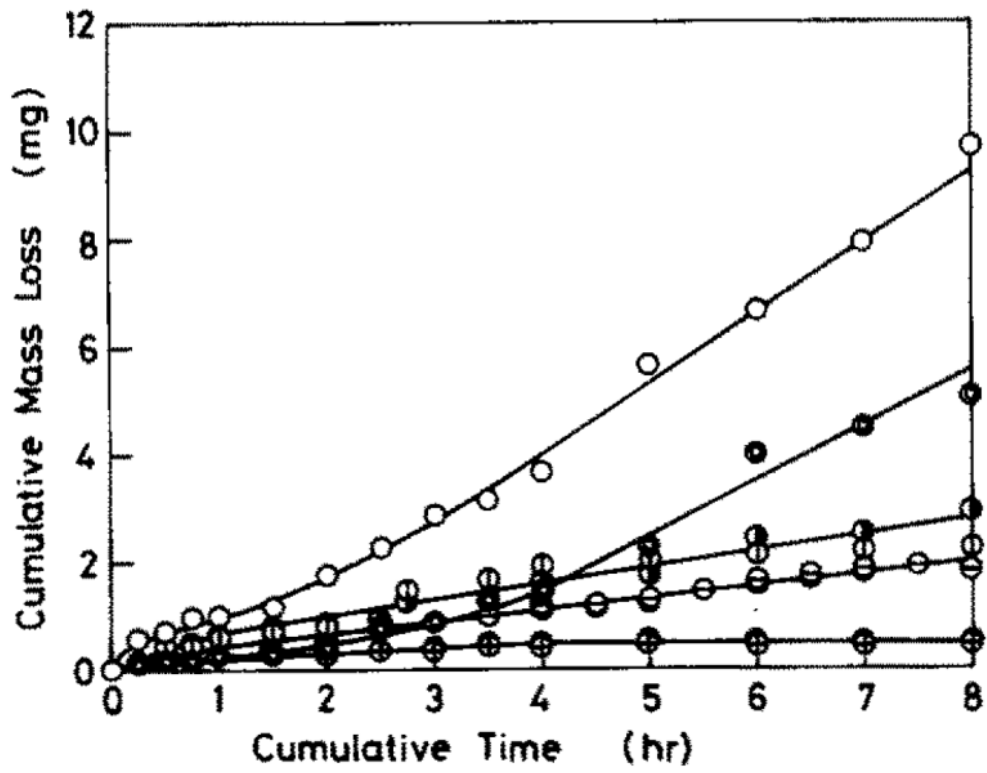


Figure 4. Temperature at the bottom of the crud for different crud thicknesses, at different bulk water boron concentrations (26).



σ	Symbol for the following specimens	
	Specimen 1	Specimen 2
0.62	⊙	○
0.70	⊖	●
0.80	⊕	⊙
0.85	⊗	●

Figure 5. Cumulative mass loss vs. time ($V = 49.0$ m/s) (28).

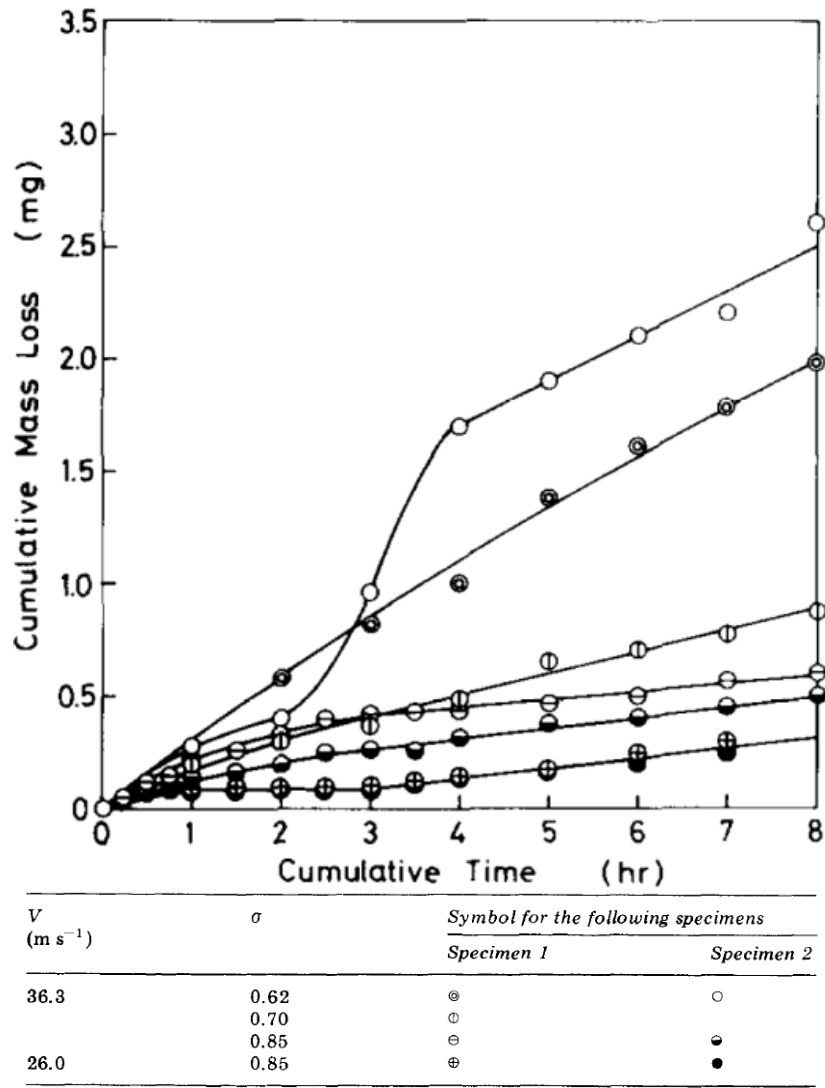


Figure 6. Cumulative mass loss vs. time ($V = 36.3$ and 26.0 m/s; uncertainty in cumulative mass loss, ± 0.05 mg) (28).

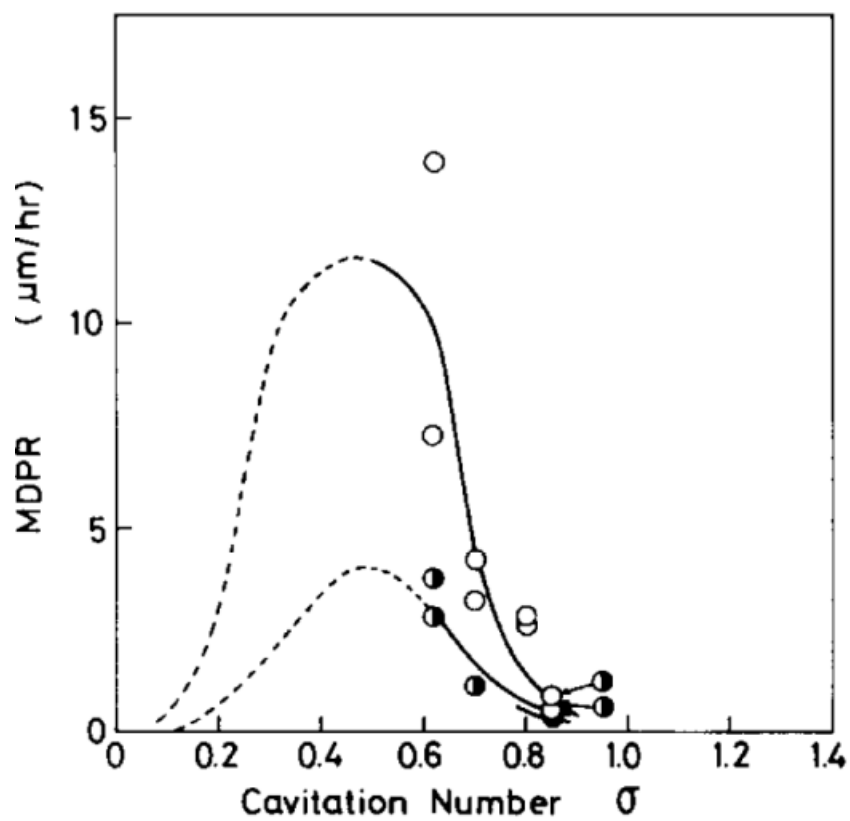


Figure 7. Effect of cavitation number σ on the MDPR (uncertainty in MDPR, $\pm 0.2 \mu\text{m/h}$): ○, $V = 49.0$ m/s; ◐, $V = 36.3$ m/s; ●, $V = 26.0$ m/s (28).

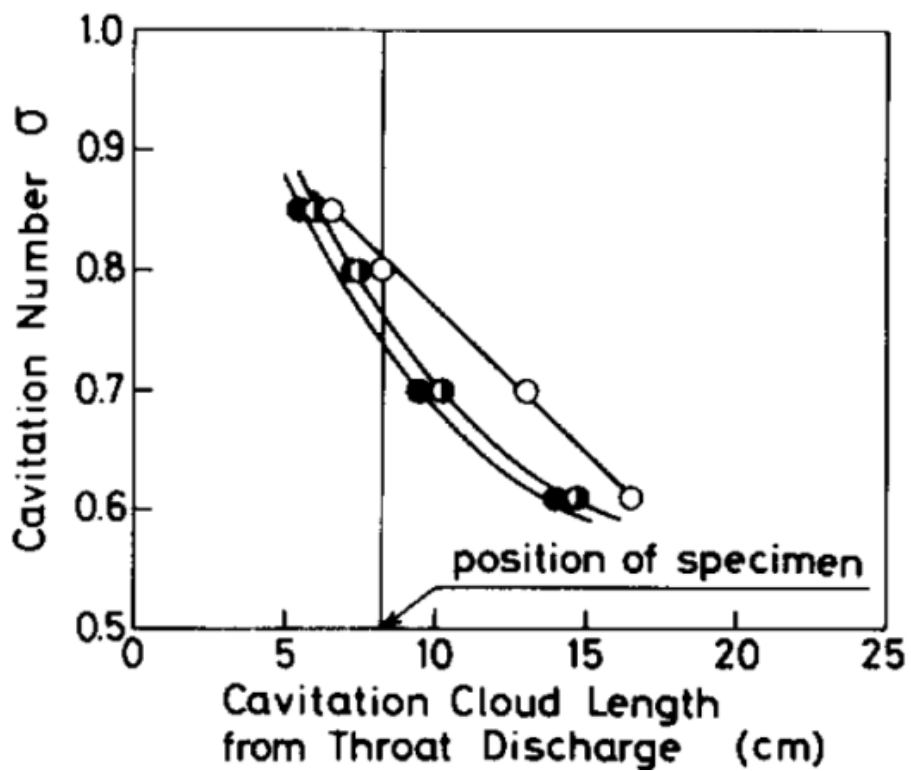


Figure 8. Cavitation cloud length vs σ (uncertainty in cloud length, ± 1 cm): \circ , $V = 49.0$ m/s; \bullet , $V = 36.3$ m/s; \bullet , $V = 26.0$ m/s (28).

PART A. Nanofluid on Reflood Heat Transfer

III. Experiments of Reflooding on Long Vertical Tube

3.1 Preparation of Nanofluids

GO/water and SiC/water nanofluid are prepared by dispersing GO and SiC nanoparticles into water as a base fluid. GO nanoparticles in this study were manufactured by the method of chemical vapor deposition (CVD). Chemical vapor deposition method is a chemical process used to manufacture high purity and performance materials and to produce thin films. SiC nanoparticles in this work were manufactured by Sigma Aldrich Corporation (true density = 3,160 kg/m³, thermal conductivity = 490 W/(mK)). It is well-known that the properties of the nanofluids depend on the shape and size of nanoparticles. To identify the morphology of nanofluids, SEM and transmission electron microscopy (TEM) images are acquired. As shown in the images of Figure 9. and Figure 10., we identified that GO nanoparticles have the shape of the plate and the thickness of one layer is less than 1 nm and SiC nanoparticles have a spherical shape. Their size is less than 100 nm.

The process of preparation of nanofluids is as follows: (1) weigh the mass of nanoparticles by a digital electronic balance; (2) put nanoparticles into the weighed water and prepare the nanoparticles/water mixture; (3) sonicate the mixture continuously for 12 hours with sonicator to obtain uniform dispersion of nanoparticles in water. Through this preparation, the temperature of nanofluids increases from 24 °C to 55 °C.

GO/water and SiC/water nanofluid were fabricated in 0.01 volume fraction (%). These values are calculated by the following conversion formula and this conversion formula is used conventionally, as it is very difficult to measure the precise volume of nanoparticles (5).

$$\varphi = \frac{1}{\left(\frac{1-\varphi_m}{\varphi_m}\right) \frac{\rho_p}{\rho_f} + 1} \quad (1)$$

Where, φ_m is the mass concentration of nanoparticles, ρ_p is the density of nanoparticle and ρ_f is the density of base fluid.

In terms of the colloidal stability or stable nanoparticles-dispersion, zeta potential is a key parameter. Zeta potential of GO/water and SiC/water nanofluids was -31.5 mV (Figure 11.) and -37.3 mV (Figure 12). It may say that these values are moderate stability, because the absolute values of zeta potential are larger than 30 mV.

In terms of the colloidal stability or stable nanoparticles-dispersion, pH is a key parameter that is related to the electrostatic charge on the particles surface. This can be interpreted and quantified as zeta potential. It is well-known that the pH value needed to maintain the stability must be far from the isoelectric point (IEP), which is the pH at which a particle surface carries no net electrical charge

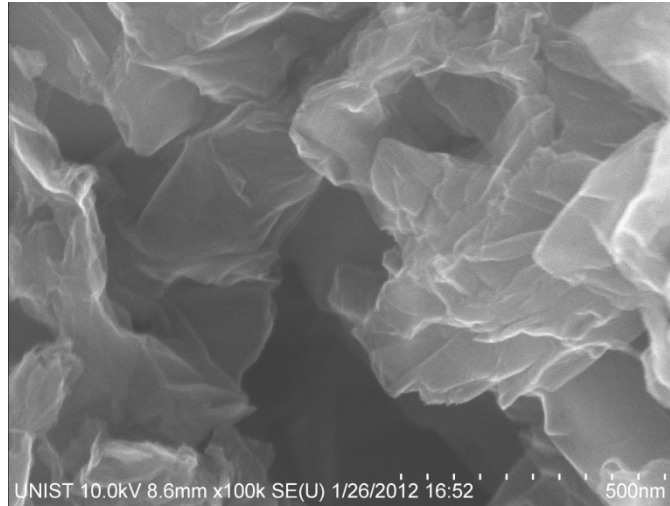
(zero zeta potential). Therefore, in a colloidal dispersion, the IEP brings about the precipitation and agglomeration of particles because there are no sufficient repulsive forces between the particles. As the pH changes from the IEP, the absolute value of the zeta potential of the particle surface increases so that the interaction between particles due to the existence of the electrical double layer (EDL) becomes sufficient to prevent attraction and collision between particles caused by Brownian motion.

3.2 Reflood Test

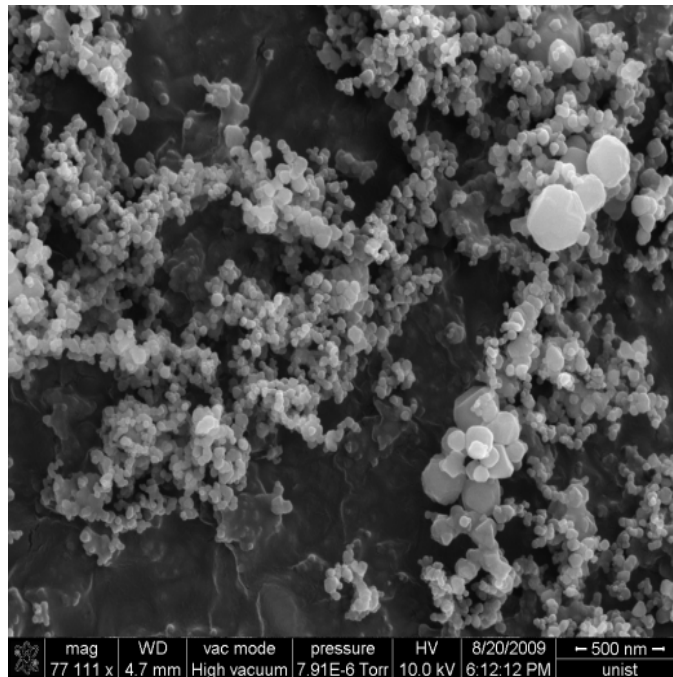
Figure 5 shows the reflood test apparatus. The test section is made of SS 316 tube (the inner diameter: 10.206 mm and the heating length: 1,300 mm), and are directly heated by a direct current passing through the tube wall. The test section is wrapped with a glass fiber insulator. Fiber glass consists of extremely fine glass fibers and is one of the most commonly used insulation materials. In order to measure the tube wall temperature, the ten K-type ungrounded thermocouples (TCs) with a sheath outer diameter of 0.5 mm are attached to the outer wall surface at intervals of 118 mm (the uncertainty of the thermocouples was ± 0.1 °C).

The main components of the experimental system include a working fluid tank, a pump with a variable speed driver to circulate the working fluids, a flow meter to confirm the flow mass rate of the working fluid (the uncertainty of the flow mass rate was less than ± 3 %), a test section, a drain tank and a DC power supply. The test section was electrically heated directly by a 4.5 kW (30 V, 150 A) DC power supply (the uncertainty of power supplied to the test section was measured less than 2 % with the multimeter). Also, an Agilent data acquisition system was used to read the individual instrument outputs and translate them into physical parameters. A computer was used to sample all the data periodically and to monitor the experiment.

The experimental procedure is as follows. The test section was heated up to between 620 °C ~ 720 °C (The standard TC is second TC from below and this was heated up to almost 720 °C), and then the cold working fluids (water and nanofluids) at 25 °C in the coolant reservoir were injected into the test section by the pump. Just before the working fluids reached the first TC, the DC power supplied to the tube was switched off. The injection flow rate (3 cm/s) was controlled by pump and the needle valve in the upstream of the test section. The total amount of each fluid was 2 liters. Two runs of the experiment were performed for each condition (water and nanofluids).

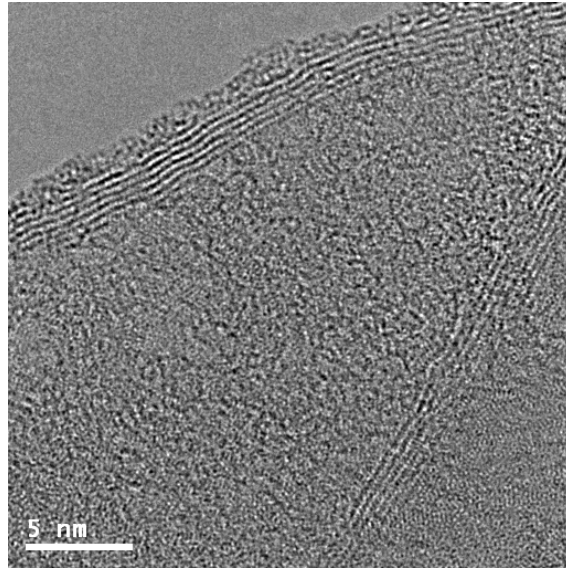


(a)

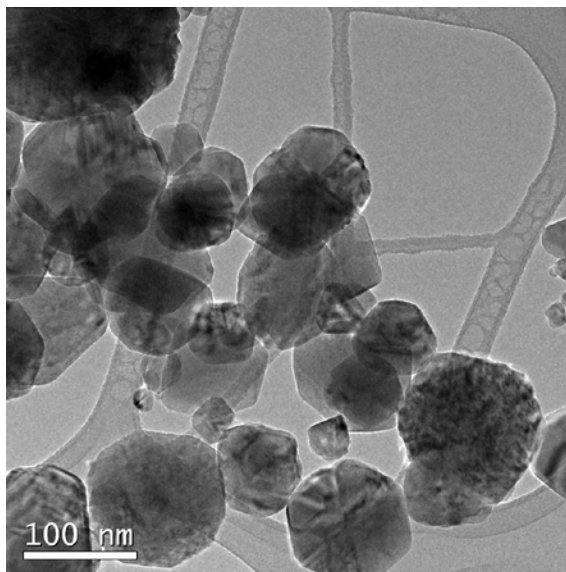


(b)

Figure 9. SEM images of nanoparticles : (a) GO and (b) SiC.



(a)



(b)

Figure 10. TEM images of nanoparticles : (a) GO and (b) SiC.

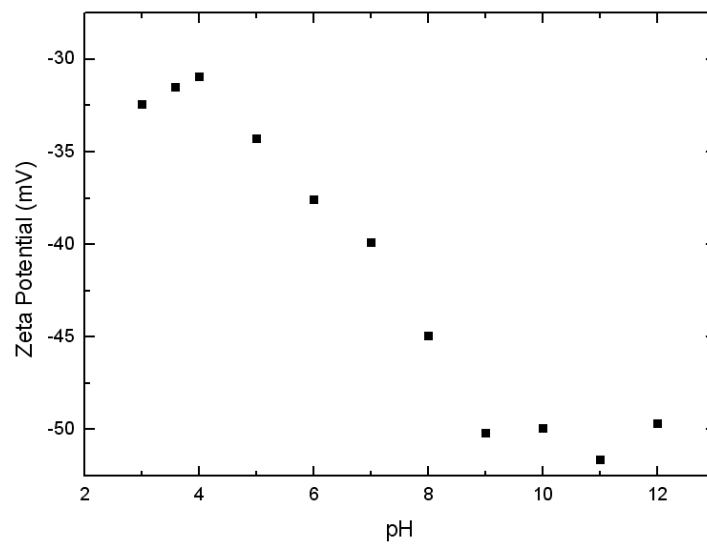


Figure 11. Zeta potential as a function of pH in case of GO/water nanofluid.

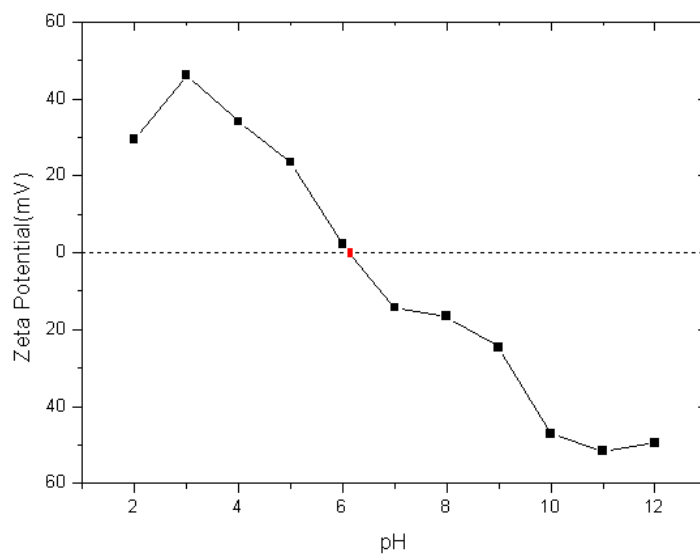


Figure 12. Zeta potential as a function of pH in case of SiC/water nanofluid.

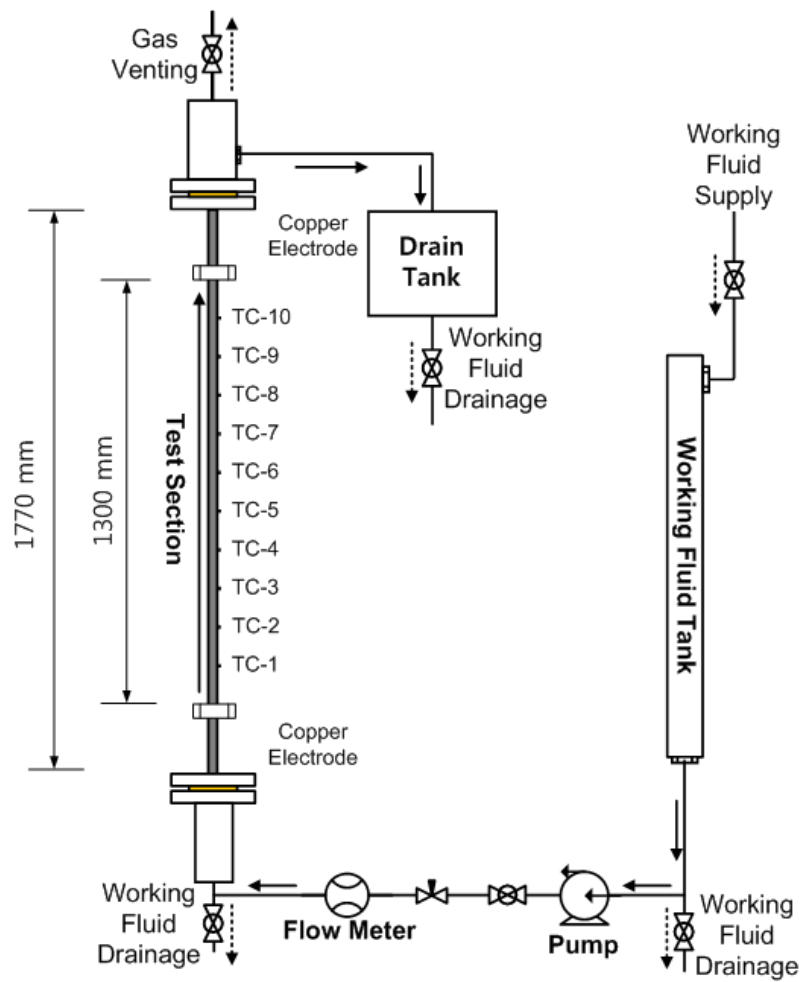


Figure 13. The reflow test apparatus.

IV. Results and Discussion

4.1 Comparison of Quenching Performance

The injection flow rate may vary during a reflood, since a phase change of the coolant and a back pressure in the test section occur. To minimize variation of the injection flow rate, the pump was used instead of nitrogen gas pressure. The injection flow rate did not vary in this experiment.

The wall temperature behavior for SiC/water nanofluid reflood was compared with that for the water reflood. Figure 14, 15 and 16 show the wall temperature variations for repetitive runs during water, SiC/water nanofluid and GO/water nanofluid refloods when the injection flow rate is 3 cm/s. As shown in Figure 14, 15 and 16, the wall temperature with two runs of the experiment was nearly same. The shape of a cooling curve shows the various cooling mechanisms that occur during the quenching process. In general, heat transfer during quenching can be described by three governing phases: film boiling, nucleate boiling, and convective boiling. The modes of heat transfer correspond to three distinctive slopes of each curve. The film boiling phase is characterized by the formation of the vapor blanket around the hot metal. The nucleate boiling phase is characterized by boiling at the metal surface (31). The transition temperature from the film boiling phase to the nucleate boiling phase is known as the Leidenfrost temperature and is independent of the initial temperature of the metal being quenched. The convective boiling phase begins when the metal cools below the boiling point of the quenching fluid. The nucleate boiling phase to the convective boiling phase transition temperature is primarily a function of the boiling point of the quenchant. Figure 17 shows the wall temperature variations during water and SiC/water nanofluid, and Figure 18 shows the wall temperature variations during water and GO/water nanofluid. Table 1 shows the comparison of quenching time and velocity for the water, SiC/water nanofluid and GO/water nanofluid. The quenching time and velocity have two values. In order to compare the quenching time and velocity, we represented the mean value of the quenching time and velocity in Table 1. As shown in Table 1 and Figure 19, the quenching time was 20 seconds faster for SiC/water and GO/water nanofluid compared with water, showing that the cooling performance for the nanofluids was higher than that of water.

Temperature which is indicating the surface of heated wall as working fluids flow to the top shows reduced cooling time than water. The reduced cooling time is due to the deposition of entrained nanoparticle. The nanoparticles deposited on the inner surface of the test section are increased the wettability of the surface and enhanced the cooling performance.

However, the temperature of TC-10 has fallen faster than TC-9 during the reflood unlike tendency of cooling curve. Precursory evaporated vapor was condensed in the upper side. When fluid is evaporated to the upper side, vapor is not easily emitted to the outside of facility. Vapor is maintained

about under 100 °C in the upper side. Therefore, heated wall in the upper side is cooled low temperature of vapor and is condensed quickly.

4.2 Analysis of Specimens

The causes of cooling performance enhancement were investigated through macroscopic observation, SEM, contact angles and SEM EDS of the inner surface of the test section in the same manner as for nanofluids. Figure 20 shows the macroscopic observations of the inner surface of the test section after the quenching experiments with both water and SiC/water nanofluid. The macroscopic observations show the deposition of SiC nanoparticles on the inner surface of the test section. Also, as can be seen in Figure 21. SEM observations show in more detail the inner surface of the test section after the quenching experiments with both water and SiC/water nanofluid. Figure 22 shows the SEM-EDS results of the inner surface of the test section after the quenching experiments with SiC/water nanofluid in order to analyze the component. As shown in Figure 22, the components of Si and C are detected. And, Figure 23 shows the SEM-EDS results of the inner surface of the test section after the quenching experiments with GO/water nanofluid. The component of C is detected as shown in Figure 23.

In order to confirm the enhanced wettability of the liquid film on the heater surface, the contact angle is investigated as shown in Figure 24. The contact angles in the inner surface of the test section after the quenching experiment with water, SiC/water nanofluid and GO/water nanofluid are 68.2° , 51.1° and 43.1° . Table 2 shows the contact angles in the inner surface of the test section after the quenching experiment with water, SiC/water nanofluid and GO/water nanofluid. Five runs of the experiment about contact angles were performed for each condition. The contact angles in the inner surface of the test section after reflooding experiment with SiC/water nanofluid and GO/water nanofluid were the smaller than that of water. A more enhanced cooling performance is attributed to a high wettability of a thin layer formed on a heating surface by a deposition of nanoparticles. When fluids are moved from bottom to top during reflood, the vapor including nanoparticles is deposited on heating surface before fluids are moved. So, the thin layer deposited nanoparticles is formed.

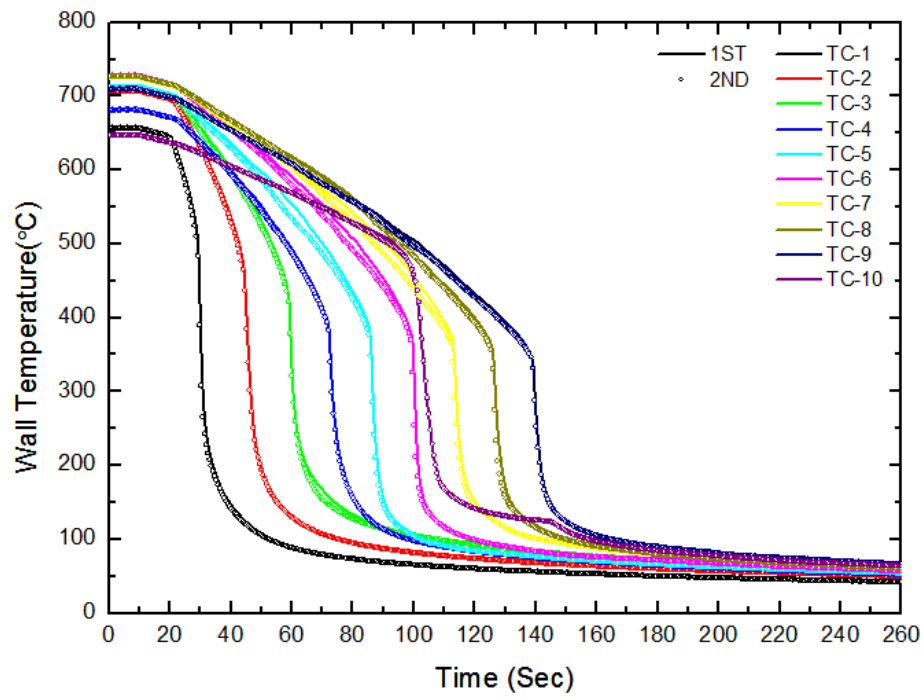


Figure 14. Wall temperature variations during water reflow.

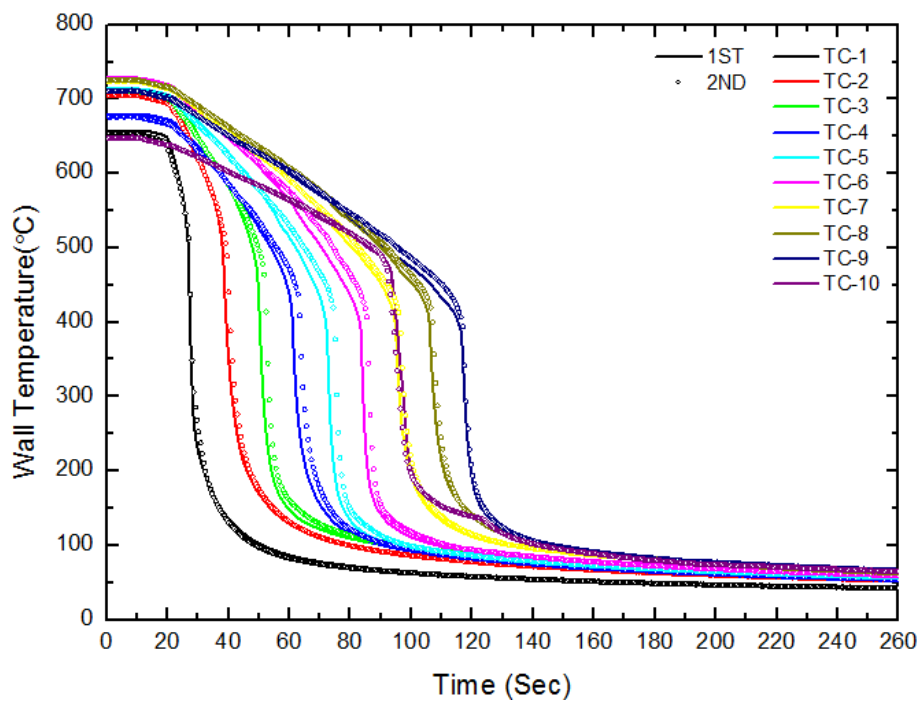


Figure 15. Wall temperature variations during SiC/water nanofluid reflow.

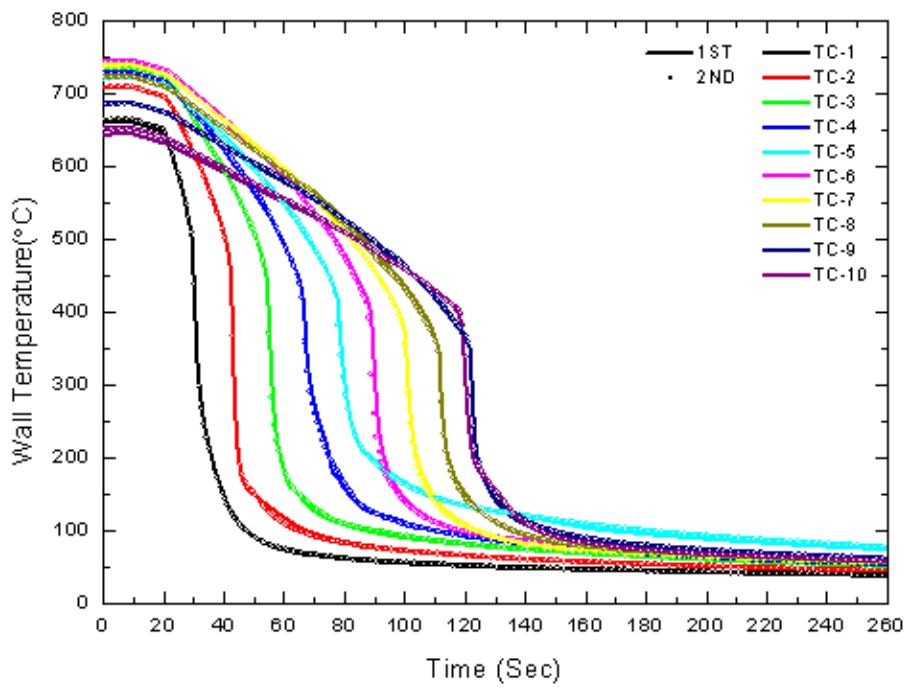


Figure 16. Wall temperature variations during GO/water nanofluid reflow.

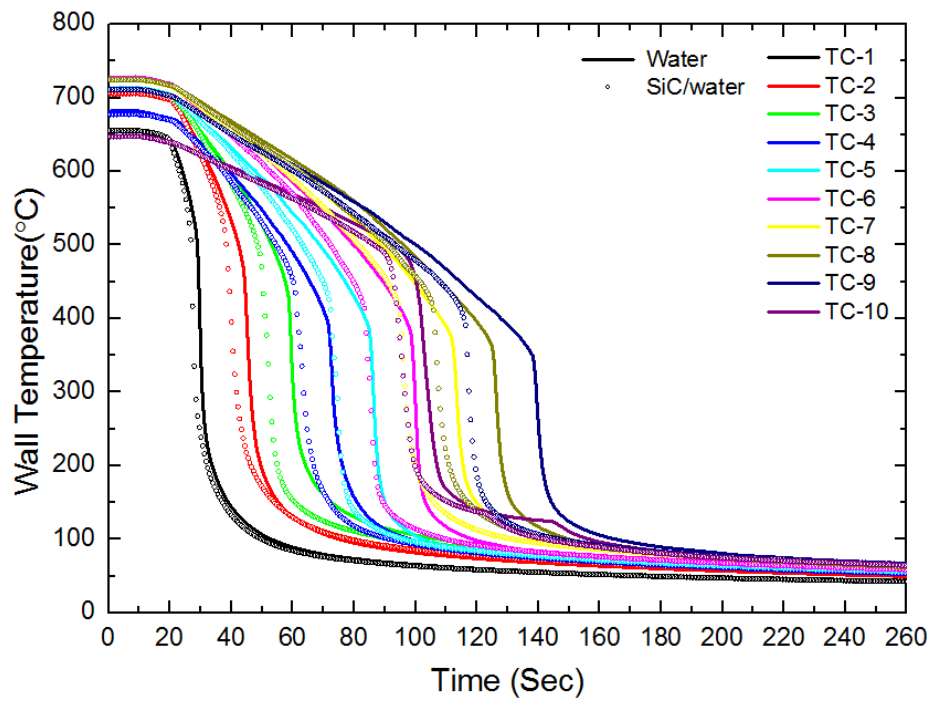


Figure 17. Wall temperature variations during water and SiC/water nanofluid.

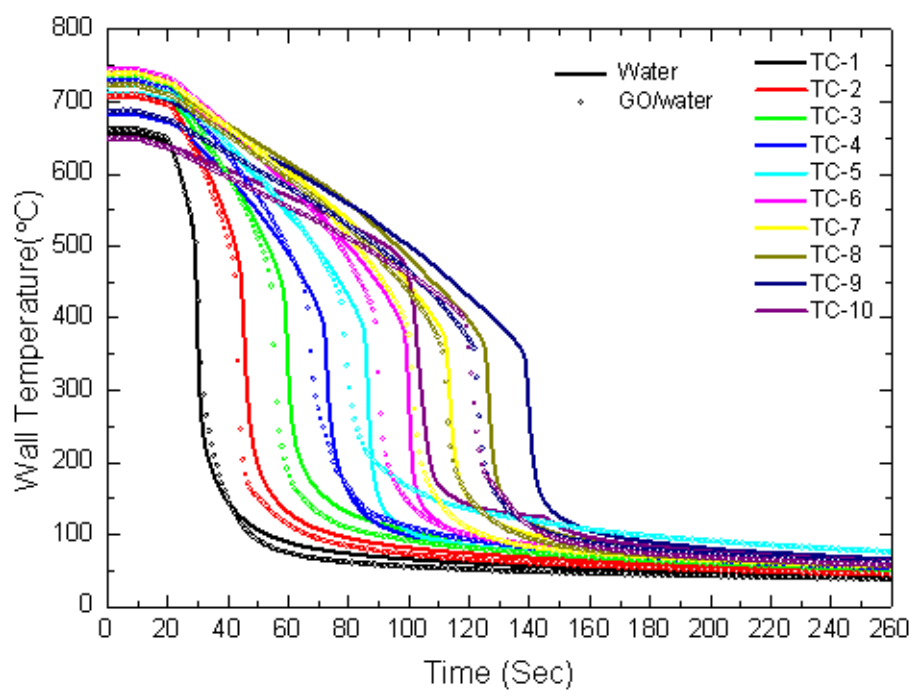


Figure 18. Wall temperature variations during water and GO/water nanofluid.

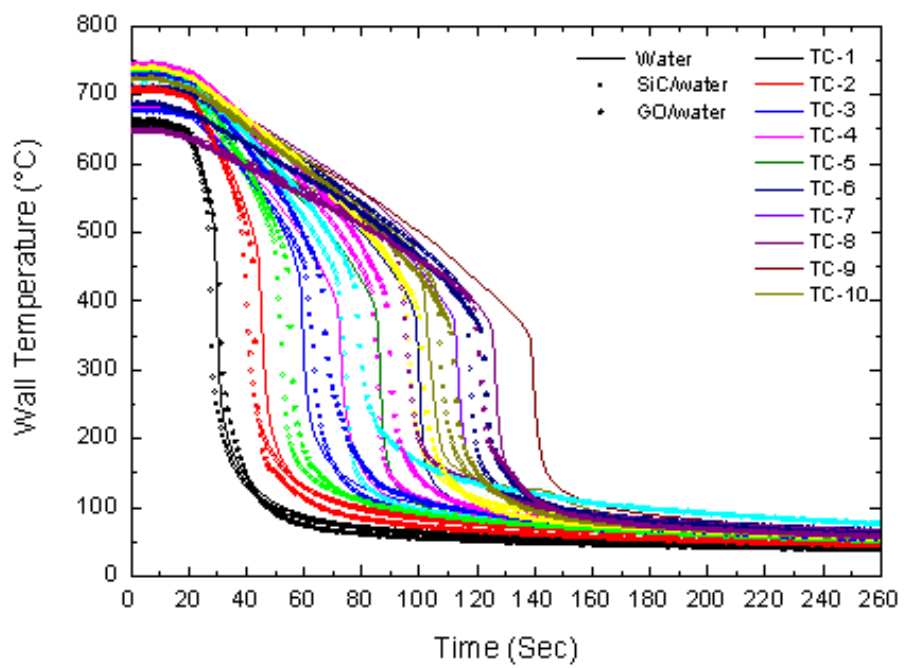


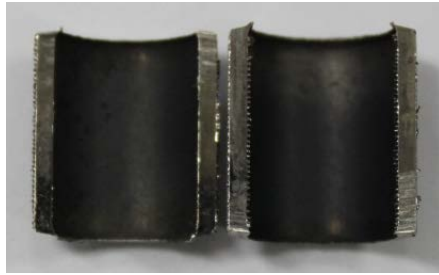
Figure 19. Wall temperature variations during water, SiC/water nanofluid and GO/water nanofluid.

Table 1. The comparison of quenching velocity during water, SiC/water nanofluid and GO/water nanofluid.

	Injection Velocity (cm/s)	Quenching Time (sec)	Average Quenching Time (sec)	Distance From TC-1 to TC-9 (cm)	Quenching Velocity (cm/s)	Average Quenching Velocity (cm/s)
Water	3	104.59	106.96	99.4	0.90	0.90
		109.34				
SiC/water Nanofluid	3	87.79	88.94	99.4	1.13	1.11
		90.09				
GO/water Nanofluid	3	88.27	90.52	99.4	1.13	1.09
		92.76				



(a)

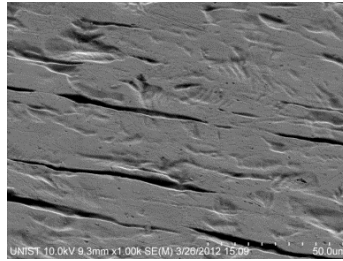


(b)



(c)

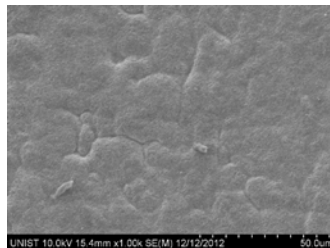
Figure 20. Macroscopic observations of the inner surface of the test section after the quenching experiments: (a) water, (b) SiC/water nanofluid and (c) GO/water nanofluid.



(a)



(b)



(c)

Figure 21. SEM observations of the inner surface of the test section after the quenching experiments: (a) water, (b) SiC/water nanofluid and (c) GO/water nanofluid.

Element	Wt%	Wt% Sigma
C	14.49	0.3
O	23.24	0.35
Si	0.34	0.06
Cr	2	0.25
Fe	59.92	0.56
Total:	100	

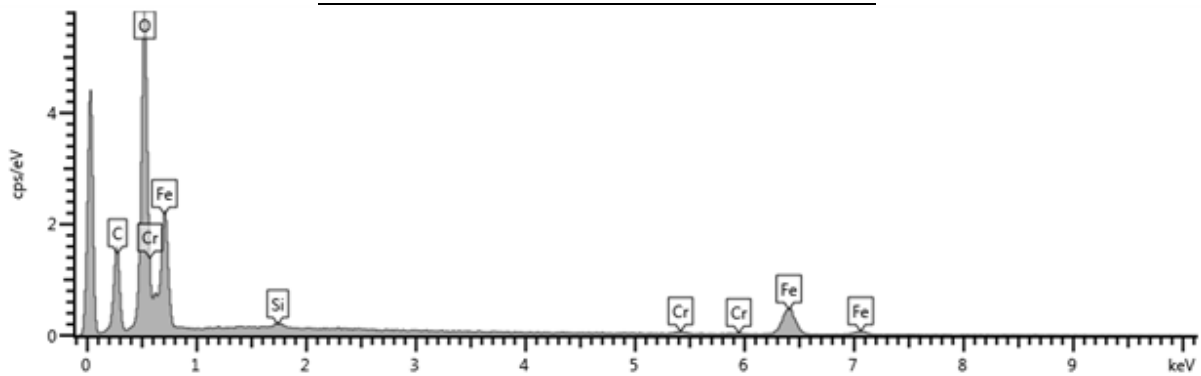


Figure 22. SEM-EDS results of the inner surface of the test section after the quenching experiments of SiC/water nanofluid.

Element	Wt%	Wt% Sigma
C	7.92	0.49
O	14.56	0.6
S	0.75	0.15
Cr	13.29	0.82
Fe	53.33	1.88
Ni	10.14	2.55
Total:	100	

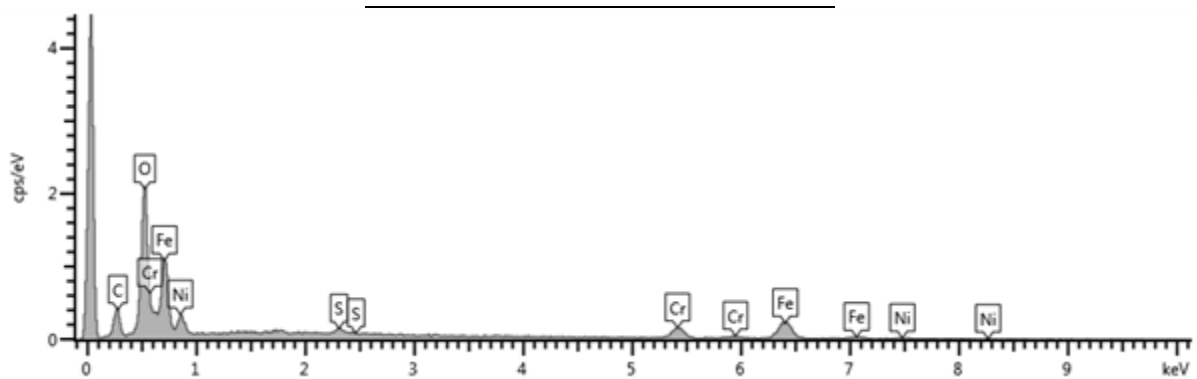
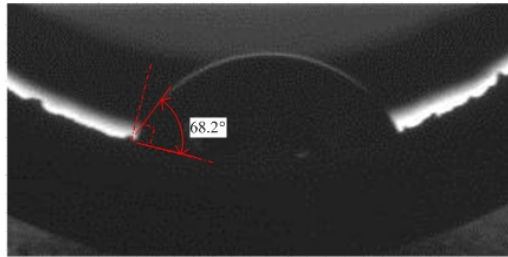
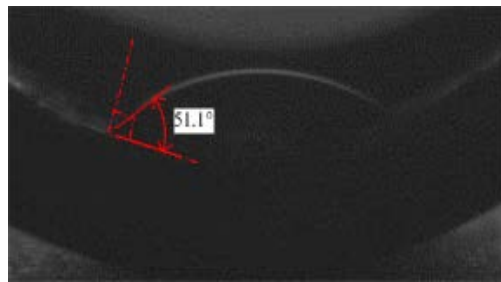


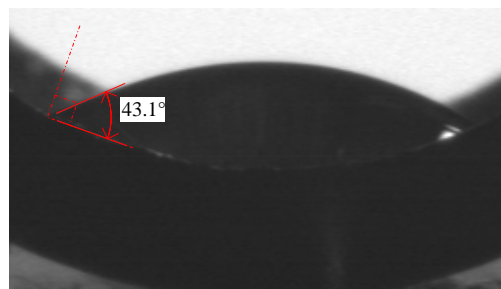
Figure 23. SEM-EDS results of the inner surface of the test section after the quenching experiments of GO/water nanofluid.



(a)



(b)



(c)

Figure 24. Contact angles of the inner surface of the test section after reflooding experiments: (a) water (68.2°), (b) SiC/water nanofluid (51.1°), (c) GO/water nanofluid (43.1°).

Table 2. Contact angles of the inner surface of the test section after reflooding experiments.

Type	Count	Angle	Average angle (°)
Water	1	70.1°	69.1°
	2	68.2°	
	3	70.7°	
	4	68.5°	
	5	68.2°	
SiC/water nanofluid	1	51.1°	51.3°
	2	51.0°	
	3	51.7°	
	4	50.5°	
	5	52.1°	
GO/water nanofluid	1	44.7°	43.4°
	2	45.4°	
	3	44.3°	
	4	43.1°	
	5	42.1°	

PART B. Hydrodynamic Cavitation on its Crud-like Deposition

V. Experiments of Hydrodynamic Cavitation

5.1 Cavitation Simulation Facility

For using the cavitation collapse pressure, an orifice is installed in the test section for a narrow fluid region as shown in Figure 25. In addition, a line static mixer was installed for the swirl flow test. Cavitation occurred at the exit of the orifice. To investigate the capacity of removal, a high speed camera recorded the cavitation phenomenon. Samples of depositions were injected into the jig holder after that holder was positioned in the test section at 2.5 D from the place of the orifice. In addition, the test section consisted of 55 mm acrylic pipe for transparency. The length of the test section is 1500 mm which consisted of 750 mm of for the front side and 750 mm for the back side, as well as an inner diameter of 55 mm. To connect the front end portion and the rear end portion of the orifice a pipe with a diameter of 14 mm is installed, when the swirl flow experiments are conducted, a line static mixer is installed on the front part of the orifice. The differential pressure caused by the orifice was measured by a differential gauge. To set up a differential pressure gauge to the position of 80 mm around each end, another pressure gauge was placed on the front side for measuring the inlet pressure. The temperature of the working fluid was indicated by thermocouples at the front of the test section and downstream of the orifice. To create the high-pressure fluid, a working fluid was supplied by a multistage centrifugal pump which has capacity of 35 m³/h of flow rate and 1.1 MPa of pumping power. The working fluids circulate from the tank to tank.

The cavitation shock pressure depends on a cavitation number. Cavitation is divided by a dimensionless cavitation number. The cavitation number is defined by the following equation:

$$\sigma = \frac{P_i - P_v}{0.5\rho v^2} \quad (4)$$

Where, σ is the cavitation number, P_i is the static pressure just downstream of the orifice, P_v is the vapor pressure of the fluid, ρ is the density of the fluid, v is the mean velocity through the orifice hole. The course of the experiment is as follows. Fluid that has passed through the orifice raises the differential pressure and generates the cavitation at the same time. At this time, shock pressure also generated by the collapse of bubbles act as a mechanism for cavitation. It is measured using a sensitive pressure film by a chemical reaction and is recorded using the high speed camera. After that,

a coated sample was tested to determine the state of cavitation as well as decontamination. During the removal, the effect of swirl flow was also performed for the study to enhance the shock pressure compared with only the orifice flow.

5.2 Preparation of Coated Specimens

Crud consists primarily of magnetite, nickel ferrite, and cobalt ferrite. For the purpose of checking the cavitation effect in this work, however, specimens made of SS 316L, an alloy of Cr, Ni and Fe are simply deposited by silicon carbide nanoparticles since the nanoparticles bond with the crud porous layer. It shows a crud-like deposition structure.

We tried to disperse the nanoparticles in the water using the quenching method, after the specimens were heated in the furnace. Complex oxide generated in the process, is judged as having a porous structure similar to crud; the experiment was done using these specimens. In this process, the adherence of the deposition was more enhanced. Figure 26 shows a polished sample sheet. For the experiments, a SS316L sheet polished by gauze grit # 800 and coated by silicon carbide nanoparticles through boiling of SiC nanofluids with a concentration of 0.1 vol % was used. The sample deposited with SiC nanoparticles is shown in Figure 27. The weight change was measured on each cavitation number using the test piece which was created by using the method previously mentioned.

5.3 Measurements of Shock Pressure

Film was used to measure the shock pressure that occurs during the collapse of cavitation. The pressure measurement film indicates an applied pressure difference as red color density variations. It is composed of a polyester base on which the color-developing material is coated, with the micro-encapsulated color-forming material layered on top. The film was discolored by the pressure with a measurement range of its own. It is individual to reflect the value stored pressure as the disposable film. For a high accuracy measurement, we use the film pressure which has a high pressure measurement range. After that, tests were conducted with film in a range of low pressure over and over again.

When the film itself reacted with water, chemical changes occur. For waterproofing, a film holder was constructed as shown in Figure 28. The holder was inserted inside the test section by inserting it after the film was injected.

VI. Results and Discussion

6.1 CFD Analysis

Prediction and analysis of the experiment was done as a CFD analysis. The swirl flow distributions through the CFD analysis were done to confirm the results obtained thereby are compared with a high-speed camera. Flows for the k- ϵ turbulence model were applied to the model in an experiment with the 1.1925 m/s conditions. The atmospheric pressure was applied to the exit. Temperature conditions were applied at a room temperature to 25 °C and CFD was used to predict the behavior of the bubble. The flow rate conditions were the same way as the entrance criteria for the test section. As a result, it showed a reflux which can be seen in Figure 29. From the exit orifice, the flow of fluid to a specific point is a reflux. In the case of swirl flow, the movement has been centralized at the exit part of the orifice.

The diameter of the orifice to the CFD is 14 mm. The specifications of the line static mixer are as follows; the length is 162 mm, and the pitch size is 480 mm. It was performed to configure the same geometry as the actual experimental conditions. The fluid that has passed through the line static mixer shows the flow of the vortex, while passing through the orifice, with the increase of flow rate, and to create a concentrated flow of fluidity. The discharged fluid in a radial direction of the orifice flow is concentrated largely by some sections of the crossover is identified as a reflux.

6.2 Image of Bubble Flow

Quantifying of bubble size of the bubbles generated by the cavitation phenomenon was conducted before to quantify the effects of cavitation. Cavitation is emitted in the radial direction around the orifice in the space filled with fluid. We can observe the increase in the size of each bubble. To investigate the bubble size, the phenomenon was recorded based on speed of the upstream by a high speed camera in each state. (The high speed camera speed is 3400 frames/sec). In an analysis of bubble distribution at each state, the results show a variable size of cavitation bubbles. Even if the state had the same conditions, the bubble size was not consistent.

Despite the image of the bubbles in the same field, the area of each bubble has various distributions. 10 samples from each area to identify through the bubble size were used as shown in Figure 30. It was calculated by the scaling method. The bubble size was reduced by increasing the flow rate and increasing the differential pressure at each state. The size of the bubble showed a large deviation as shown in Figure 31, even under the same conditions and location.

6.3 Pressure Film

We measured the cavitation number according to pressure film for accurate control over cavitation. Next we used pressure film for measuring the pressure. As different kinds of pressure film have different limitations, first we measured pressure by a high level pressure film, then confirmed whether it is in the proper range. If it was not in the proper range, we measured pressure by a low level pressure film. We also measured pressure film that is not exposed to cavitation for considering the effect of pressure by a holder in measuring pressure. As a result of measuring pressure by a holder, there were effects of pressure by the O-ring in circumference and via cutting. As a result we ruled out the effects of that when measuring the effects of cavitation. Figure 32 shows the result of shock pressure when forming cavitation using only an orifice without the line static mixer. It shows the highest shock pressure when the cavitation number is 0.5. The pressure value is in inverse proportion to the cavitation number and Figure 33 shows the result of pressure when forming cavitation in swirl flow conditions using an orifice and line static mixer. The pressure value is also in inverse proportion to the cavitation number. Effect of cavitation is shown in Table 3 and Table 4. Table 6 show the data of shock pressure at the cavitation flow, and it was compared with results between our experiment and other author's experiment on the cavitation flow to analyze the difference. If we consider only the orifice flow, shock pressure values were slightly larger than other experiments at each cavitation. In order to compare the results, results are obtained in the orifice facility and consider the ratio of the orifice diameter as shown in Figure 34.

6.4 Sample Test

The weight change was measured through each coated sample. The samples coated with 1 mg of nanoparticles were exposed to cavitation at the same time, and it was compared with the results between using an only orifice and using both an orifice and line static mixer. In order to confirm the removal effects by cavitation, experiments were conducted using SiC coated samples in various ranges of flow. In this experiment, we fix the flow velocity and the pressure in the proper cavitation number. Samples are inserted in to the holder then the amount of removed surface materials were confirmed by weight change. Table 5 shows the result. It was eroded actively when the cavitation number was 0.6.

Comparison of each sample shows the difference tendency of weight change. At cavitation number 0.6, specimen is actively eroded than other condition. And, above the cavitation number 0.7, we could not see the difference in the specimens. It shows the difference results when weight change was compared with other results, our results doesn't have any tendency in this test. Because collapse of cavitation bubble clusters was observed at different position, erosion effect can vary from cavitation number. Cavitation bubble clusters, termed as cavitation cloud, shows different length at the each cavitation number. Length of cavitation cloud was in proportion to cavitation number. So, it doesn't make the tendency of the erosion effect at each position along the cavitation number. Therefore, our experiment was shows different result when it is compared to the venturi test (25). Our results of erosion effect may be verified by another orifice test (29).

Table 3. Effect of cavitation on the orifice.

Mass flow rate (kg/s)	Differential Pressure (MPa)	Equipment type	Time	Cavitation number	Max pressure (MPa)
2.76	0.49	Orifice	5 min	0.5	37
2.65	0.44	Orifice	5 min	0.6	31
2.53	0.40	Orifice	5 min	0.7	12

Table 4. Effect of cavitation in combination with the orifice and static mixer.

Mass flow rate (kg/s)	Differential Pressure (MPa)	Equipment type	Time	Cavitation number	Max pressure (MPa)
2.83	0.51	Orifice + Mixer	5 min	0.5	63.8
2.66	0.43	Orifice + Mixer	5 min	0.6	23.3
2.50	0.38	Orifice + Mixer	5 min	0.7	5
2.33	0.32	Orifice + Mixer	5 min	0.8	0.9
2.16	0.27	Orifice + Mixer	5 min	1	0.95

Table 5. Erosion effect of cavitation in combination with the orifice and static mixer.

Cavitation number	Equipment type	Time	Weight change
0.8	Orifice	15 min	0.1 mg
	Orifice + Static mixer		
0.7	Orifice	15 min	0.1 mg
	Orifice + Static mixer		
0.6	Orifice	15 min	0.3 mg
	Orifice + Static mixer		
0.5	Orifice	15 min	0.2 mg
	Orifice + Static mixer		

Table 6. Shock pressure at the cavitation number on each experiment (27),(32).

	Pipe diameter (mm)	Orifice diameter (mm)	Ratio of the orifice diameter (d/D)	Velocity of throat (m/s)	Shock pressure (MPa)	cavitation number
					32	0.4
Takahashi et al. (27)	76.2	28	0.37		24	0.5
					8	0.8
Nagaya et al. (32)	49.5	24.75	0.5	15.3	4.7~5.9	0.7
					12	1.2
				17.9	37	0.5
Experiment	55	14	0.3	17.2	31	0.6
				16.4	12	0.7

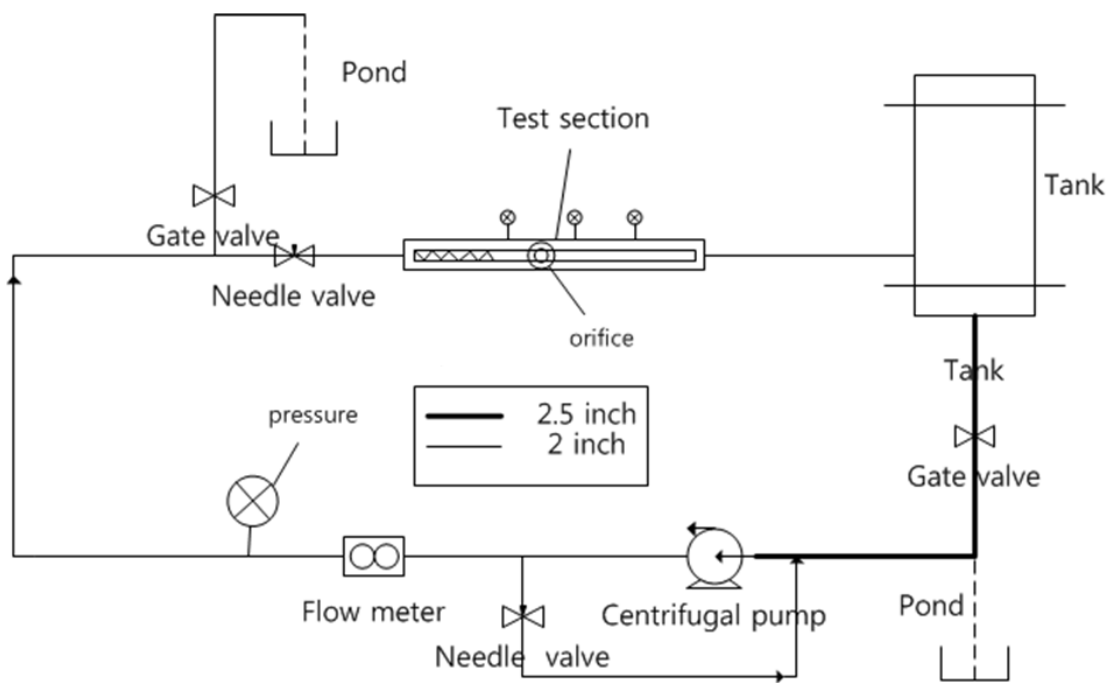
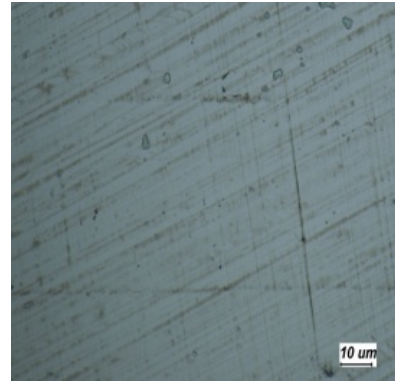


Figure 25. Schematic of experiments.



(a)

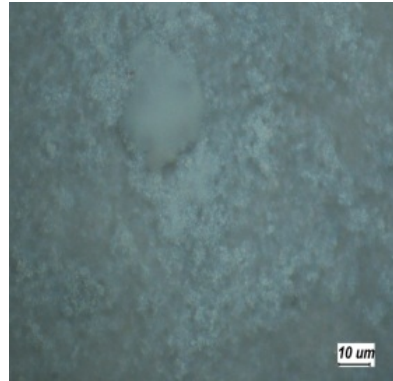


(b)

Figure 26. Bare sample: (a) optical image, (b) microscope image of 1,000x magnification.



(a)



(b)

Figure 27. SiC-coated sample: (a) optical image, (b) microscope image of 1,000x magnification.

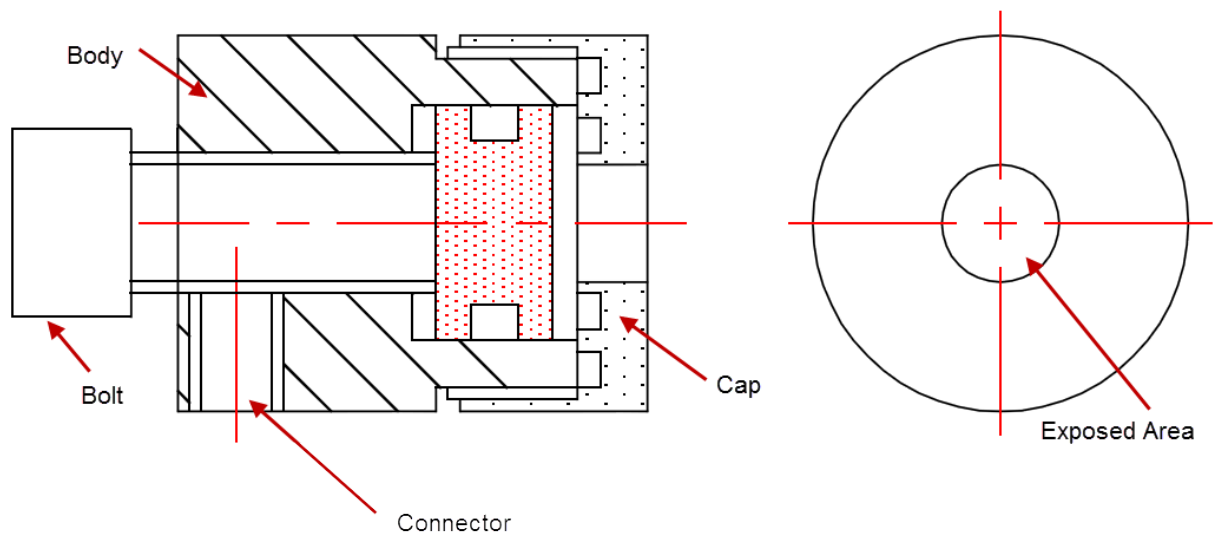


Figure 28. Film holder.

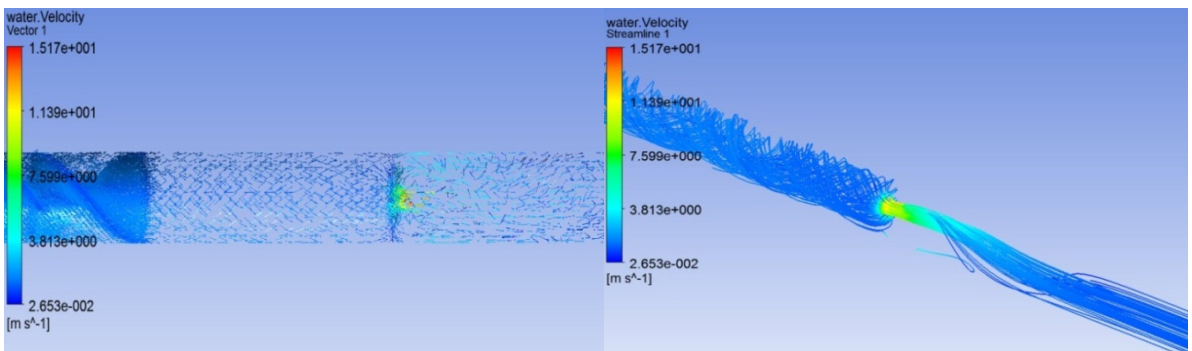


Figure 29. Analysis of flow by CFD.

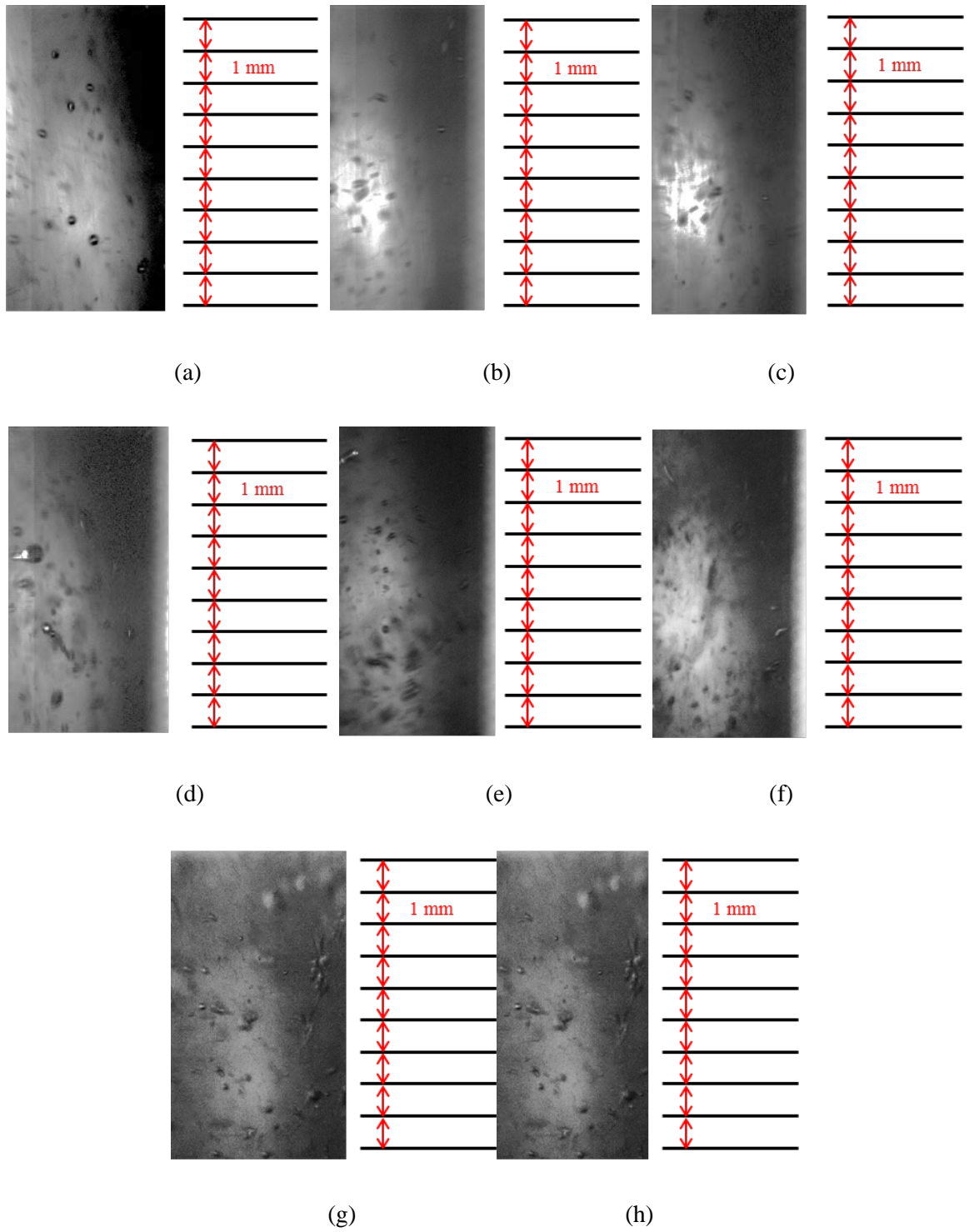


Figure 30. Bubble distribution and size at each flow state: (a) $V : 9.54 \text{ m/s}$, $DP: 1.830 \text{ bar}$; (b) $V : 10.27 \text{ m/s}$, $DP : 1.570 \text{ bar}$; (c) $V : 11.01 \text{ m/s}$, $DP: 1.798 \text{ bar}$; (d) $V : 11.74 \text{ m/s}$, $DP: 1.993 \text{ bar}$; (e) $V : 12.48 \text{ m/s}$, $DP: 2.287 \text{ bar}$; (f) $V : 13.21 \text{ m/s}$, $DP : 2.541 \text{ bar}$; (g) $V : 13.95 \text{ m/s}$, $DP: 2.876 \text{ bar}$;

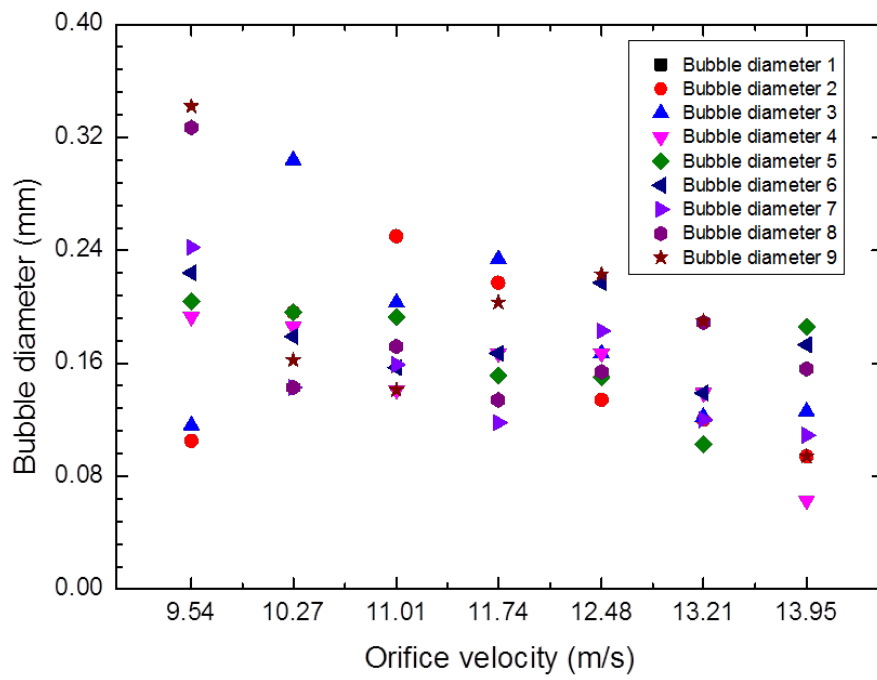


Figure 31. Bubble size distribution.

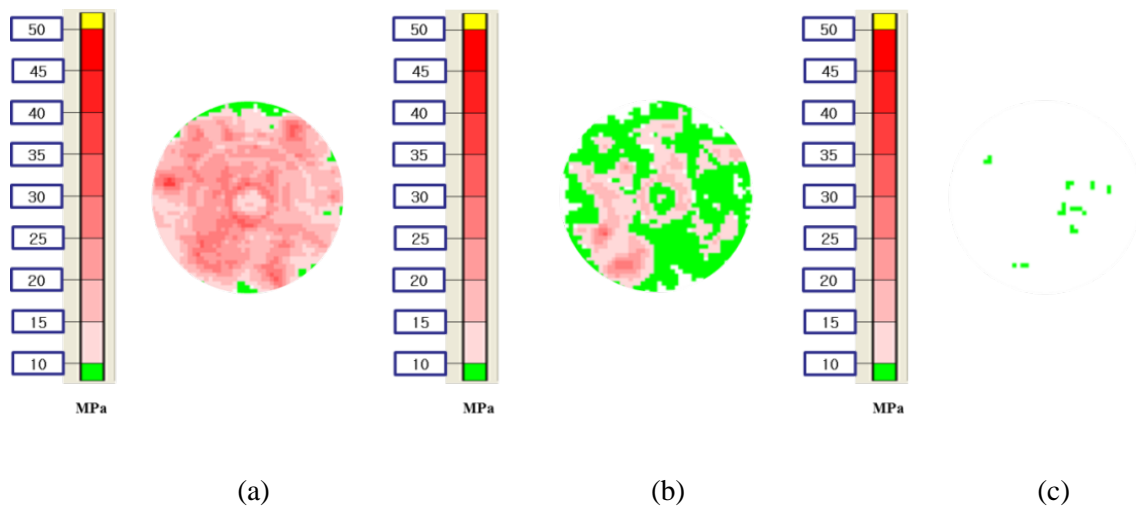


Figure 32. Effect of cavitation number in cases of using the orifice: (a) $\sigma = 0.5$, (b) $\sigma = 0.6$, (c) $\sigma = 0.7$.

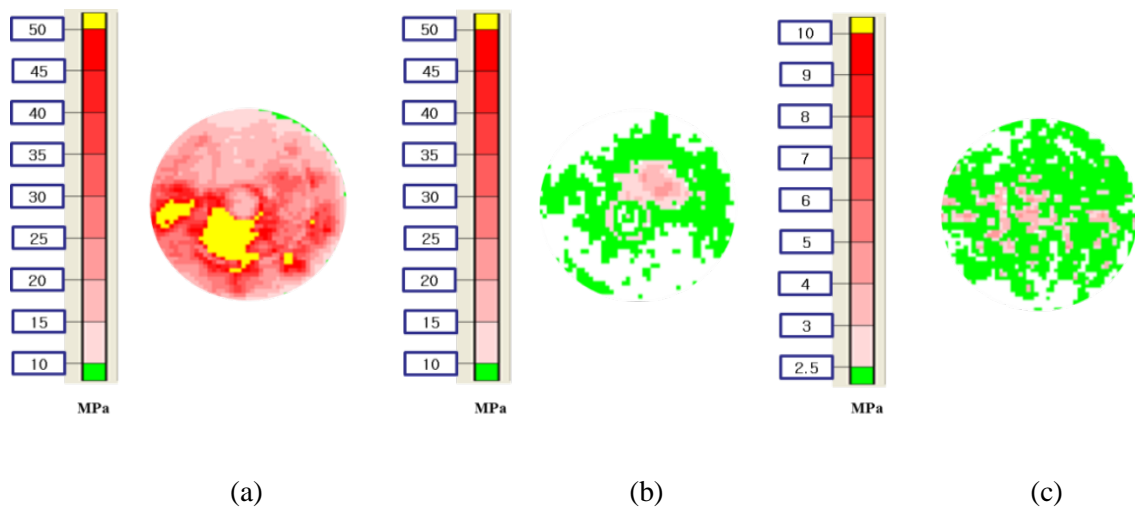
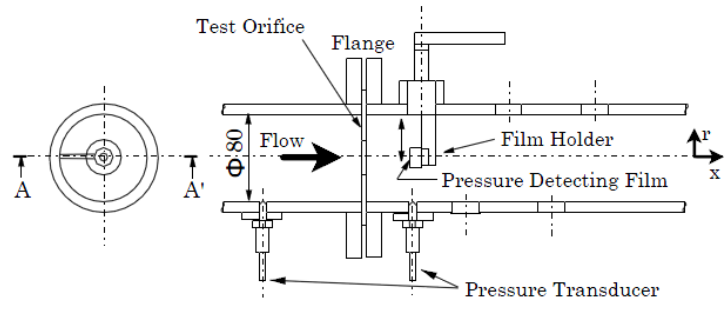
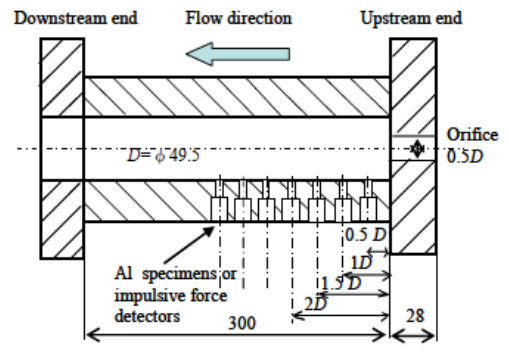


Figure 33. Effect of cavitation number in cases of using a combination of orifice and mixer: (a) $\sigma = 0.5$, (b) $\sigma = 0.6$, (c) $\sigma = 0.7$.



(a)



(b)



(c)

Figure 34. Compared each test section: (a) Takahashi et al. (27), (b) Nagaya et al. (32), (c) Our experiment (27),(32).

VII. Summary and Conclusions

SiC nanoparticles has the high thermal conductivity. This is considered one of the strong candidates to function as cladding material of the fuel rod in advanced and fusion reactor. If it is used as suspended material in the coolant, it can dedicate to reduce and recover the damage on the fuel under the nuclear accident. And, if we consider specimens SiC coated, the removing of the coated surface by cavitation phenomenon can be confirmed to the weight loss induced by erosion effect. Moreover, the fuel rod coated SiC nanoparticle as results of circulated SiC nanoparticle can verify how to bear the cavitation. So, selection of SiC nanoparticle can attribute to ensure the safety in the nuclear power plant. Graphene oxide has been studied to apply to many research fields because of its high thermal conductivity. Therefore, dispersed GO particles can attribute the high cooling performance in this work. These experiments are firstly researched using the SiC/water and GO/water nanofluids on the reflow system in the long vertical tube. It can attribute to accelerate the performance of coolant by adding some material. Another research of cavitation experiment using the specimens SiC coated is studied to remove the crud. In addition, this test can attribute the verification of resistance of cavitation on the SiC cladding. Moreover, it can be helpful to remove the undesired coated layer. Our researches can be helpful to these motivations. Results of our experiment can help the adoption of nanoparticle. Results are as follows:

For reflooding experiments,

The present works were conducted to investigate the effect of nanofluids on reflow heat transfer in a long vertical tube. When the potential application of nanofluids comes to ECCS, the situation of interest is quenching phenomena of fuel rods during reflow of emergency coolants. The following results are obtained.

- (1) The reflow tests have been performed using nanofluids as a coolant, instead of water. We have observed an enhanced cooling performance in the case of the nanofluid reflow.
- (2) A cooling performance is enhanced more than 20 seconds for SiC/water nanofluid and GO/water nanofluid.
- (3) A more enhanced cooling performance is attributed to a high wettability of a thin layer formed on a heating surface by a deposition of nanoparticles. The enhancing cause of the cooling performance after the quenching experiments using the nanofluids were investigated through macroscopic observation, SEM, contact angles and SEM-EDS of the inner surface of the test section.

- (4) The increase of quenching velocity for nanofluids is attributed to rupture of vapor blanket/film due to turbulence enhancement.
- (5) At the severe accident, a more enhanced cooling performance can be a decreased amount of hydrogen. So, this can reduce the degree of hydrogen explosion.

For cavitation experiments;

Hydrodynamic cavitation generates the shock pressure of a few tens MPa due to bubble collapse. It is well known that the cavitation can erode the metal surface. The study of cavitation on crud-like deposition presents much interest because such energetic cavitation bubble collapses could help to remove the crud from the fuel assembly. Additionally, the following results are obtained.

- (1) In comparison with bubble containing different cavitation numbers, each bubble has a different diameter. In the case of the same cavitation number, the bubble's diameter is varied. So using a mean of diameter is required.
- (2) In experiments using cavitation, cavitation can get rid of nano crud layers partially but cannot remove layers that were made through a method in high adhesiveness over a short time. Consequently, a long term experiment is essential for inspection over an experiment using cavitation.
- (3) In certain distances from the end of the orifice, the majority of bubbles cannot be observed and are formed around the orifice. For using cavitation accurately, the nozzle diameter should be considered.
- (4) Following the result of measuring shock pressure according to the cavitation number through pressure film, the highest pressure is observed when the cavitation number is 0.5. There is no relation between the cavitation number and pressure at a cavitation beyond 0.8.
- (5) Measured pressures in two types of flows, the higher pressure levels are observed in cases when using a line static mixer. Shock pressure becomes linear when the bubble collapses by swirl flow. This seems like the result of shock pressure when the bubble collapses by swirl flow.
- (6) Shock pressure by pressure film shows a high mean pressure in the orifice flow.
- (7) Result of the CFD analysis and images through the high-speed camera, a flow through orifice are turned to a backward flow at a certain distance from the end of the orifice. It can cause the probability of high shock pressure. Reflux disturbs the movement that is extending the residence time of bubble in the flow.

Our researches can contribute to understand the behavior of entrainment. In other experiment, almost of quenching experiments were conducted using the sphere and short rodlet. Therefore it has the limitation to simulate the sub-channel. Our experiments use the long vertical tube. So, it can more attribute to understand the nanofluid effect.

Cavitation experiment using the SiC coated specimens on each cavitation number is useful to analyze the damage of SiC cladding when it was exposed to cavitation. And, it can be useful to remove the undesired crud coated surface. And results of SiC performance attribute to understand the potential usage of SiC cladding.

VIII. Acknowledgement

During my stay at UNIST, I have met many people who gave good impacts to my life.

I am deeply grateful my thesis advisor, Professor In Cheol Bang, for his guidance and unwavering support to me throughout my stay at UNIST. I owe special thanks to my thesis committee members, Professor Ji Hyun Kim and Professor Hyung Wook Park for their advice that helped me bring my research to final fruition.

I sincerely thank to my laboratory colleagues. I want to thank them for all their help, support, interest and valuable advice. Especially I am obliged to Seung Won Lee, Seong Dae Park, Sarah Kang, Han Seo, Dong Han You, Byeong Jin Choi, Sang Hun Shin, Jong Jin Kim, Ju Ang Jung, Tae Woo Tak, Ju Yeong Lee, Kyoung Jun Choi, Sang Il Choi.

Lastly, thanks to my family for their great support and help to accomplish this study. They are the cornerstone in my life. They were always cheering me up and stood by me through the good and bad times.

Reference

1. Choi, S. U. S., Nanofluids: from vision to reality through research. *Journal of Heat Transfer* **2009**, *131*, 033106.
2. Xuan, Y.; Li, Q., Heat transfer enhancement of nanofluids. *International Journal of Heat and Fluid Flow* **2000**, *21* (1), 58-64.
3. You, S.; Kim, J.; Kim, K., Effect of nanoparticles on critical heat flux of water in pool boiling heat transfer. *Applied Physics Letters* **2003**, *83* (16), 3374-3376.
4. Vassallo, P.; Kumar, R.; D'Amico, S., Pool boiling heat transfer experiments in silica–water nano-fluids. *International Journal of Heat and Mass Transfer* **2004**, *47* (2), 407-411.
5. Bang, I. C.; Heung Chang, S., Boiling heat transfer performance and phenomena of Al₂O₃–water nano-fluids from a plain surface in a pool. *International Journal of Heat and Mass Transfer* **2005**, *48* (12), 2407-2419.
6. Kim, H.; Kim, J.; Kim, M., Experimental Study on CHF Characteristics of Water-TiO₂ Nano-Fluids. *Nuclear engineering and technology* **2006**, *38* (1), 61.
7. Kim, S. J.; Bang, I. C.; Buongiorno, J.; Hu, L. W., Surface wettability change during pool boiling of nanofluids and its effect on critical heat flux. *International Journal of Heat and Mass Transfer* **2007**, *50* (19–20), 4105-4116.
8. Maxwell, J. C., *A treatise on electricity and magnetism*. Clarendon Press: 1881; Vol. 1.
9. Park, H. S.; Shiferaw, D.; Sehgal, B.; Kim, D. K.; Muhammed, M. In *Film boiling heat transfer on a high temperature sphere in nanofluid*, Proceeding of the ASME Heat Transfer/Fluids Engineering Summer Conference: Volume 4, 2004; pp 469-476.
10. Lotfi, H.; Shafii, M., Boiling heat transfer on a high temperature silver sphere in nanofluid. *International Journal of Thermal Sciences* **2009**, *48* (12), 2215-2220.
11. Kim, H.; DeWitt, G.; McKrell, T.; Buongiorno, J.; Hu, L., On the quenching of steel and zircaloy spheres in water-based nanofluids with alumina, silica and diamond nanoparticles. *International*

Journal of Multiphase Flow **2009**, 35 (5), 427-438.

12. Kim, H.; Buongiorno, J.; Hu, L. W.; McKrell, T., Nanoparticle deposition effects on the minimum heat flux point and quench front speed during quenching in water-based alumina nanofluids. *International Journal of Heat and Mass Transfer* **2010**, 53 (7), 1542-1553.
13. Chun, S. Y.; Bang, I. C.; Choo, Y. J.; Song, C. H., Heat transfer characteristics of Si and SiC nanofluids during a rapid quenching and nanoparticles deposition effects. *International Journal of Heat and Mass Transfer* **2011**, 54 (5), 1217-1223.
14. Bolukbasi, A.; Ciloglu, D., Pool boiling heat transfer characteristics of vertical cylinder quenched by SiO₂-water nanofluids. *International Journal of Thermal Sciences* **2011**, 50 (6), 1013-1021.
15. Ciloglu, D.; Bolukbasi, A., The quenching behavior of aqueous nanofluids around rods with high temperature. *Nuclear Engineering and Design* **2011**, 241 (7), 2519-2527.
16. Lee, S. W.; Chun, S. Y.; Song, C. H.; Bang, I. C., Effect of nanofluids on reflood heat transfer in a long vertical tube. *International Journal of Heat and Mass Transfer* **2012**.
17. Murao, Y., Correlation of quench phenomena for bottom flooding during loss-of-coolant accidents. *Journal of Nuclear Science and Technology* **1978**, 15 (12), 875-885.
18. Kim, A.; Lee, Y., A correlation of rewetting temperature. *Letters in Heat and Mass Transfer* **1979**, 6 (2), 117-123.
19. Duffey, R.; Porthouse, D., The physics of rewetting in water reactor emergency core cooling. *Nuclear Engineering and Design* **1973**, 25 (3), 379-394
20. Lee, R.; Reyes, J. N.; Almenas, K., Size and number density change of droplet populations above a quench front during reflood. *International Journal of Heat and Mass Transfer* **1984**, 27 (4), 573-585.
21. Dougall, R. S.; Rohsenow, W. M. *Film boiling on the inside of vertical tubes with upward flow of the fluid at low qualities*; Cambridge, Mass.: Dept. of Mechanical Engineering, Massachusetts Institute of Technology, [1963]: 1963.

22. Groeneveld, D.; Moeck, E. *An investigation of heat transfer in the liquid deficient regime*; Atomic Energy of Canada Ltd., Chalk River (Ontario). Chalk River Nuclear Labs.: 1969.
23. Richlen, S.; Condie, K., Comparison of post-CHF heat transfer correlations to tube data. *INEL, SRD-134-76, Idaho Falls, Idaho* **1976**.
24. Chatzikiyiakou, D.; Walker, S. P.; Hewitt, G. F., The contribution of non-wetting droplets to direct cooling of the fuel during PWR post-LOCA reflood. *Nuclear Engineering and Design* **2010**, *240* (10), 3108-3114.
25. Pan, C.; Jones, B. G.; Machiels, A. J., Concentration levels of solutes in porous deposits with chimneys under wick boiling conditions. *Nuclear Engineering and Design* **1987**, *99*, 317-327.
26. Henshaw, J.; McGurk, J. C.; Sims, H. E.; Tuson, A.; Dickinson, S.; Deshon, J., A model of chemistry and thermal hydraulics in PWR fuel crud deposits. *Journal of nuclear materials* **2006**, *353* (1), 1-11.
27. Takahashi, K.; Matsuda, H.; Miyamoto, H. In *Cavitation characteristics of restriction orifices*, Proc. of 4th international symposium on cavitation, CAV, 2001.
28. Hattori, S.; Sun, B. H.; Hammitt, F. G.; Okada, T., An application of bubble collapse pulse height spectra to venturi cavitation erosion of 1100-o aluminum. *Wear* **1985**, *103* (2), 119-131
29. Fan, M.; Tao, D.; Honaker, R.; Luo, Z., Nanobubble generation and its application in froth flotation (part I): nanobubble generation and its effects on properties of microbubble and millimeter scale bubble solutions. *Mining Science and Technology (China)* **2010**, *20* (1), 1-19.
30. Vickers, G.; Houlston, R., Modelling the erosion efficiency of cavitation cleaning jets. *Applied scientific research* **1983**, *40* (4), 377-391.
31. Totten, G. E.; Bates, C. E.; Clinton, N., *Handbook of quenchant and quenching technology*. ASM International (OH): 1993.
32. Nagaya, Y.; Murase, M.; Mizuyama, S.; Hattori, S., Evaluation of Incipient Cavitation Erosion on Pipe Walls Downstream from an Orifice. *Journal of Environment and Engineering* **2010**, *5* (2), 389-401.